THE INFLUENCE OF MICROENVIRONMENT ON NEURAL PROGENITOR CELLS IN HEALTHY AND DISEASED STATES

Research Project Major Thesis, University of Groningen, Research Master Behavioral and Cognitive Neuroscience, N-Track: Molecular and Cellular Neuroscience

Aleksandra Cywinska, s4058100

Prof. Amalia Dolga, Dr. Marina Trombetta-Lima.
Molecular Pharmacology, University of Groningen

ABSTRACT

Microenvironment plays a big role in modulating cellular behavior. Especially in the case of stem cells, proliferation and fate determination is largely influenced by extracellular cues. Moreover, in neurodegenerative diseases such as Alzheimer's Disease, the neurodegeneration often occurs alongside a pre-determined anatomical order – possibly due to different cellular composition and extracellular matrix (ECM) features in different brain regions. Here, we focused on investigating the influence of scaffold composition, ultrastructure and stiffness on the neuronal progenitor cells (NPCs) morphology, proliferation and differentiation. To investigate that, we wanted to compare the influence of ECM obtained from different brain regions on NPCs derived from induced pluripotent stem cells (iPSCs) from AD patients (with the PSEN1 mutation) and controls. To assess the cellular interaction with the scaffold, NPCs were seeded on 3D porous nanostructures of two different scales coated with laminin. Separately, we also tested hydrogels of varying stiffnesses and we worked on optimizing the procedure for region-specific brain decellularization. Our preliminary data show that NPCs seeded in stiffer gels display higher proliferation while the morphology of the cells is more elongated in softer gels. The first seeding of NPCs on the scaffolds showed that they are able to interact with it and enter the inner structures, provided the pores are large enough. Our results will help clarify the mechanisms by which the microenvironment modulates progenitor cell niche in neurodegeneration.

Table of Contents

INTRODUCTION

Microenvironment plays a crucial role in modulating cellular behavior, constituting about 20% of the brain (Pavlov, Lauri, Taira, & Rauvala, 2004). This is especially true for stem cells which develop into specific lineages depending on the inductive cues around them. At the same time, the microenvironment is a key mediator of disease progression, including in the cases of neurodegeneration (Sachs, Mollica, & Bruno, 2017). Alzheimer's Disease (AD) is a common neurodegenerative disorder with increasing prevalence due to the growing population of individuals over 60 years of age (Prince et al., 2015). Two of the most prominent pathophysiological features of the disease are the extracellular amyloid beta plaques and the intracellular neurofibrillary tangles, which lead to increasing loss of neurons, and consequentially episodic memory deficits, visuo-spatial disturbances and other cognitive dysfunctions (McCoy & Tansey, 2008). While plaques and tangles have independent spatio-temporal paths, the anatomical route of each of these pathologies is relatively coherent among patients, starting usually in the medial temporal area (Braak & Braak, 1991). Therefore, certain characteristics of the microenvironment in these regions could be influencing the cells with certain genetic predispositions to develop in a pathological way.

Neural progenitor cells (NPCs), which give rise to neurons and astrocytes, are themselves grown from induced pluripotent stem cells (iPSCs) which are directly generated from patients and healthy individuals. Here we have used this as our experimental model since it allows for detailed examination of the differences between affected and healthy states at a molecular and cellular level. Both NPCs and the differentiated astrocytes and neurons generated from AD patients have different characteristics than those of healthy controls, such as decreased renewal of progenitor cells, as well as altered metabolism and cytokine production (Meyer et al., 2019; Oksanen, Petersen, Naumenko, Puttonen, Lehtonen, Olivé, et al., 2017).

Here we aimed to investigate the importance of three aspects of the microenvironment: scaffold composition, ultrastructure and stiffness. We examined their influence on the morphology, proliferation and differentiation of NPCs derived from healthy controls and AD patients with PSEN1ΔE9 mutation.

Composition

The extracellular matrix (ECM) is the non-cellular part of an organ or tissue, continuously regulated *in vivo* by enzymes and mostly composed of water, proteins and polysaccharides (Fernández-Pérez & Ahearne, 2019). While the ECM varies between tissue to tissue, its composition is especially unique in the brain (Ruoslahti, 1996), where various proteins are differentially expressed throughout different areas, providing region-specific cues (Barros, Franco, & Müller, 2011). The ECM can influence intracellular signaling pathways, proliferation, migration and attachment, and is therefore a perfect scaffold for inducing and maintaining a given phenotype (Frantz, Stewart, & Weaver, 2010). Mimicking the structure and composition of the native ECM as close as possible is crucial for tissue engineering, and one of the ways of obtaining it is through tissue decellularization, which allows for removing the potentially immunogenic components (cells) while preserving the structure and desirable biochemical cues of the ECM. Such acellular tissue has proven effective as a matrix for tissue engineering from various organs, such as lungs, skin, skeletal muscle and liver cells (Cortiella et al., 2010; Zhang et al., 2009).

Given the unique composition and structure of central nervous system's (CNS) ECM, it is not surprising that brain-derived scaffolds have been shown to have a different influence on cells than the non-CNS ones (Crapo et al., 2012). Neurons, glial cells and neural stem cells are known to express receptors allowing them to interact with ECM molecules such as proteoglycans, tenascins and laminins (Barros et al., 2011). ECM is crucial for all kinds of processes happening in the brain, from neural stem cell differentiation and migration to synaptic functioning (Zimmermann & Dours-Zimmermann, 2008). In order to investigate the differential influence of culturing NPCs in ECM derived from specific brain areas, we decellularized fragments of a porcine brain and obtained region-specific matrix.

3D Structures

While the biochemical composition of the ECM is important, the structural organization is also crucial in defining cellular behavior, serving as a scaffold for adhesion, proliferation and migration (Granato et al., 2020). Contrary to growing cells on a plate, neurons in the brain grow within a complex 3D matrix composed of thin fibers synthesized from ECM proteins (Antonova, Kochetkova, & Shlyapnikov, 2021). Such fibrous structures have been found in decellularized

brain tissue, and mimicking those would create microenvironment even closer to that of a native brain (DeQuach, Yuan, Goldstein, & Christman, 2011).

Here we have conducted preliminary analysis on the influence of artificially created 3D scaffolds on NPCs differentiation and proliferation. The scaffold's microporous structure and channels enable interactions between cells which can themselves provide crucial cues in the differentiation process (Onesto, Accardo, Vieu, & Gentile, 2020). Additionally, the cube-like structure adopted here allows for nutrients delivery to the inside parts of the growing network, ensuring minimal cell death.

Stiffness

Stiffness of a biomaterial can be defined as the rigidity with which it is resisting deformation as a result of applying a given force (Fan, Staufer, & Accardo, 2019). Changes in matrix stiffness can influence the differentiation processes of human mesenchymal stem cells towards either neuronal or glial cells (Her et al., 2013). Moreover, it has recently been shown that even at the embryonic state the stem cell fate determination is influenced by not only chemical but also mechanical forces, for example stiffness (Thompson et al., 2019).

Additionally, changes in the mechanical property of tissues are a known phenomenon in various disorders, e.g. cancers – with the tumors being usually stiffer than normal tissue (Fiore et al., 2020). On the other hand, the brains of AD patients are on average softer than those of healthy controls (Hiscox et al., 2020). This change is evident both on a whole-brain and regional level (mostly in temporal lobe). Specifically, the reduction in stiffness of the hippocampus was found to be as high as 22% (Gerischer et al., 2018). This difference in stiffness could influence neurogenesis and contribute to the accelerated neuronal differentiation, reduced cell renewal and differences in the astrocytes/neuronal ratio of AD-derived NPCs (Meyer et al., 2019). Through culturing such NPCs in hydrogels of varying stiffnesses we wanted to investigate what influence will this aspect of the microenvironment have on the cellular phenotype and morphology.

Experimental Design

We obtained the ECM from different porcine brain regions through means of chemical decellularization with detergents. Porcine brain ECM has been found to be an alternative to Matrigel for human cerebral organoid formation as the cells showed comparable gene expression and differentiation processes (Simsa et al., 2021). It has also shown good cell attachment and growth capabilities (Reginensi et al., 2020). The decellularized matrix was then lyophilized and the DNA content was quantified in order to assess the efficacy of the procedure.

For structural analysis we have used two different scales of 3D structures which were made from stiff acrylate polymer and contained curved unit pores of various sizes. We seeded NPCs derived from a healthy individual and an AD patient to optimize the size and characteristics of the scaffolds, as well as to investigate their potential interaction and its influence on the morphology of the cells. We have used the NPCs from patients with presenilin-1 (PSEN1ΔE9) mutation which is a subunit of gamma secretase responsible for the generation of amyloid beta plaques from the amyloid precursor protein (Grimm, Rothhaar, & Hartmann, 2012).

To investigate the effect of stiffness on NPCs differentiation and proliferation we have used hydrogels of varying stiffnesses created from either alginate (natural polysaccharide) or gelatin (collagen-derived protein). We then seeded NPCs generated from a healthy individual in these hydrogels in order to investigate their morphology after two weeks of differentiation.

METHODS

The induced pluripotent stem cells (iPSCs) lines used in this study were previously generated from two healthy volunteers and three Alzheimer Disease patients with the PSEN1 Δ9 mutation (Oksanen, Petersen, Naumenko, Puttonen, Lehtonen, Gubert Olivé, et al., 2017). Neural Progenitor Cells (NPCs) were generated according to previously published protocols (Gunhanlar et al., 2018).

Decellularization (Composition)

Dissected fragments of porcine brain were stored at -80°. After thawing in PBS, the initial weights were measured and the tissue fragments were cut into smaller pieces with a scalpel. They were then incubated for 1h at RT on agitation in 1% Triton X-100 (Sigma Aldrich, #X100)

in deionized water. The procedure was repeated if necessary, until tissue turned orange-white (Fig. 1B vs Fig. 1A). Then the tissue was incubated in 2% sodium deoxycholate (Sigma-Aldrich, #D6750) in deionized water for 1-2h at RT on agitation. This process was repeated until complete decellularization occurred (Fig. 1C). For overnight storage, pieces were put in PBS and kept at 3 degrees. Decellularized matrix was stored in Eppendorf tubes at -20°. The samples were then lyophilized, weighed and stored at -20° until further use.

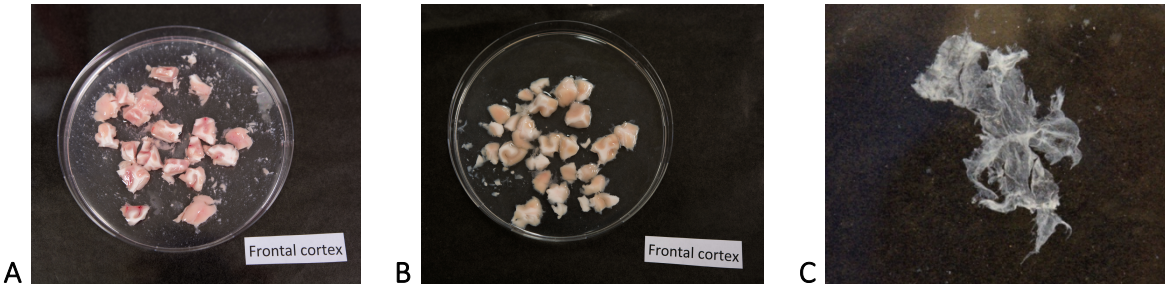

Fig. 1 Pictures of the decellularization process **A** Day 1: Freshly thawed and cut tissue **B** Day 2: The same tissue after 1.5h incubation in Triton X-100 **C** An example of a fully decellularized tissue fragment

DNA QUANTIFICATION. In order to quantify the efficiency of the decellularization process we measured the DNA content of the decellularized matrix and compared it to the original tissue's content. We used 12.5 mg of frontal cortex tissue, both pre- and post-decellularization. The DNA isolation was performed with QIAzol Lysis Reagent (Qiagen, #436178564) as indicated in the manufacturers protocol (MAN0016385). The obtained DNA samples were then quantified using the NanoDrop Spectrophotometer (ND-1000).

Media and Reagents

NPCs were grown on laminin-coated flasks (20 µg/ml; Cultrex #3400-010-02) in Advanced DMEM/F12 Medium (Gibco, #12634-010) supplemented with 1% N2 Supplement (Gibco, #17502048), 2% B27 neural supplement minus Vitamin A (ThermoFisher, #12587010), 1 µg/ml laminin, 20 ng/ml FGF (Peprotech, #100-18B) and 1% penicillin/streptomycin solution (Gibco, #15070-063). Medium was changed every 3-4 days and cells were passed with 0.5ml of collagenase type IV 1000 U/mL (Thermo Fisher; #17104019). To induce differentiation, the medium was changed to the BrainPhys Neuronal Medium (Stem Cell Technologies, #05790) supplemented with 1% N2 supplement, 2% B27 supplement minus Vitamin A, 1% MEM Non-Essential Amino Acid Solution (Gibco, #11140050), 20 ng/ml BDNF (Peprotech, #450-02), 20

ng/ml GDNF (Peprotech, #450-10), 1 µM db-cAMP (Sigma, #D0627) and 200 µM ascorbic acid (Sigma, #A4544).

3D Structures

The scaffolds tested in this study were generated by MSc Ahmed Sharaf (Prof. Angelo Accardo's group, TU Delft). The structures were created from a stiff acrylate polymer and had overall dimensions of around 100 µm – 100 µm – 100 µm (Fig. 2). We have tested two different scales of structures, both of which had the same overall volume and shape. The difference in the size of the inside pores between the different scales were: from 6 to 131 μm^2 for small and from 19 to 387 μm^2 for large. The rods in both cases had a diameter of 3 µm and a radius of curvature of 50 µm.

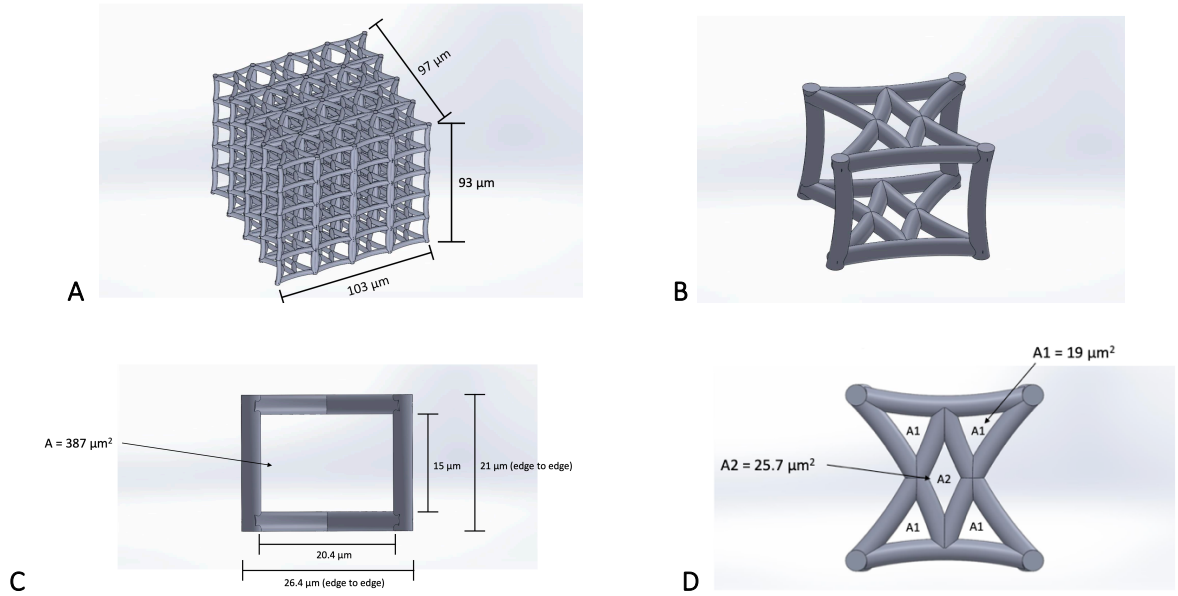

Fig. 2 Example of the large-scale structure **A** Isometric view of the whole structure **B** Isometric view of the unit cell **C** Side view of the unit cell **D** Top view of the unit cell (images provided by the collaborators)

CELL CULTURE. Scaffolds were sterilized with 70% ethanol for 15 minutes and washed three times with UP water. Structures were then coated with 20 µg/ml of laminin. Two NPCs lines were seeded on the scaffolds in the NPCs medium: one healthy control (LL90 Cl 1.5, passage 3.10), and one affected (AD2 Cl 1.3, passage 3.10), in density $21x10^4$ cells/cm^2. After one week the medium was changed to neural differentiation medium. After seven day of differentiation, cells were fixed – the scaffolds were washed three times with PBS, after which 4% PFA (Sigma-Aldrich, #158127) was added for 15 min at RT. Then cells were washed again in PBS and kept at 4°.

IMAGING. Cells were first permeabilized with 1% Triton X-100 and then washed 3 times in PBS. We then incubated them in Alexa Fluor 488 Phalloidin (1:40; Life Technologies, #A12379) and DAPI (1 µg/ml) for 1h at RT in the dark. Pictures of the cells were taken with the Leica SP8 Confocal Microscope.

Hydrogels (Stiffness)

The hydrogels tested in this study were generated and provided by Mohammad Khoonkari (Prof. Frank Kruyt & Prof. Marleen Kamperman's groups, UMCG). Two hydrogels with whole-porcine-brain ECM and different base materials were used (alginate vs gelatin). We also compared different stiffnesses of the gels, namely 0.5 kPa, 4 kPa, 2kPa and 8 kPa.

CELL CULTURE. NPCs from a healthy control line were seeded in the neuronal differentiation medium on the hydrogels with the density of $25x10^3$ cells/well (p. 3.11 for healthy LL90). The cells were seeded in a 30 µL drop of medium on top of the hydrogel-filled well and incubated for 4 to 6h for attachment, after which the plate was filled with 8 ml of differentiation medium. The cells were left in the gel for two weeks.

IMAGING. After two weeks we removed the medium, washed the samples with PBS and incubated them in 4% PFA for 15 min at RT. After fixing the cells we washed them with PBS again, and then permeabilized them with 1% Triton X-100. Cells were then washed 3 times in PBS and incubated with Alexa Fluor 488 Phalloidin (1:40) and DAPI (1 µg/ml) for 1h at RT in the dark. The images were taken with the Leika SP8 Microscope.

RESULTS

Decellularization (Composition)

To investigate the influence of brain region-specific ECM, we first had to optimize the decellularization process of the native brain tissue. We have worked with various areas of a porcine brain, which were weighted before and after the process (Table 1). The weight decreased drastically during the decellularization, to on average 7.9% of the initial one, and even further after the lyophilization.

Table 1. Decellularized brain areas and their weights.

Brain Area	Initial Weight	Weight After Decellularization	Weight After Lyophilization
Frontal 1.0	16,4 g	0,81 g (4,89%)	0,044 g
Cerebelllum	6,02 g	0,86 g (14,23%)	0,043 g
Temporal	8,14 g	0,58 g (9,23%)	0,041 g
Frontal 2.0	13,04 g	1,20 g (7,12%)	0,052 g
Insula	0,45 g	0,45 g (4,24%)	0,020 g
Thalamus	2,71 g	0,19 g (7,05%)	0,002g
Hippocampus	4,11 g	0,42 g (10,28%)	0,008 g
Medulla oblongata	1,50 g	0,13 g (8,79%)	0,001 g
Corona Radiata	3,24 g	0,15 g (4,66%)	0,010 g
Pons	2,27 g	0,19 g (8,46%)	0,011 g
Occipital	12,39 g	---	0,019 g
Parietal	11,83 g	---	0,013 g

The exact time of incubation of the tissue in sodium deoxycholate varied between tissue types and sizes, however the final stage can clearly be differentiated and decellularized matrix can be identified by eye, or when needed, by microscopy (Fig. 3).

A 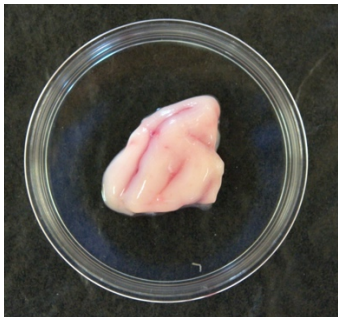 B 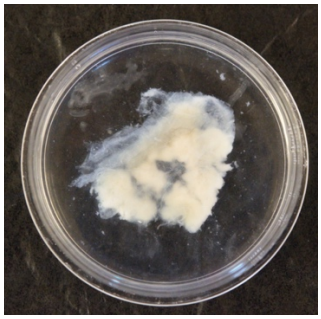 C 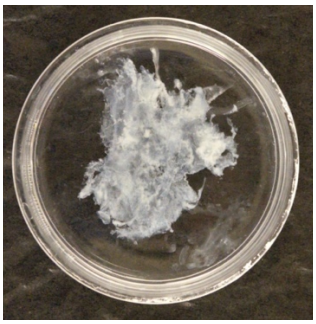

Fig. 3 Fragment of the occipital lobe throughout the decellularization process (dish ø: 60 mm) **A** Thawed tissue piece in PBS **B** The same tissue fragment after 3.5h in Triton X-100 and 15h in sodium deoxycholate **C** Occipital lobe after full decellularization: 3.5h in Triton X-100 and 23h in sodium deoxycholate

In order to assess the efficacy of the decellularization process we have performed DNA isolation with QIAzol, followed by quantification. When comparing the pre- and post-decellularized fragments of a porcine frontal cortex there was a clear decrease in the content of the DNA (see Fig. 4).

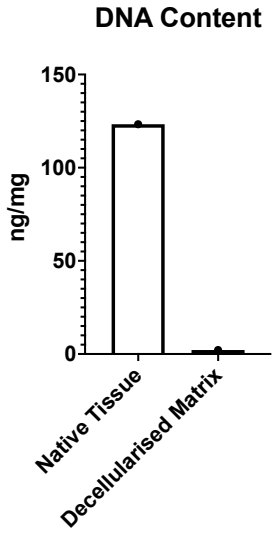

Fig. 4 DNA Content of the frontal cortex pre- and post-decellularization. Values expressed as ng of DNA/ mg of native tissue.

3D Structures

We have studied the influence of culturing NPCs on 3D structures through first optimizing their design and then investigating their interactions. We have used two cell lines for this: one affected (AD2) and one healthy (LL90), and we have noticed that the former had higher proliferation rates while the control had a more elongated morphology (Fig. 5).

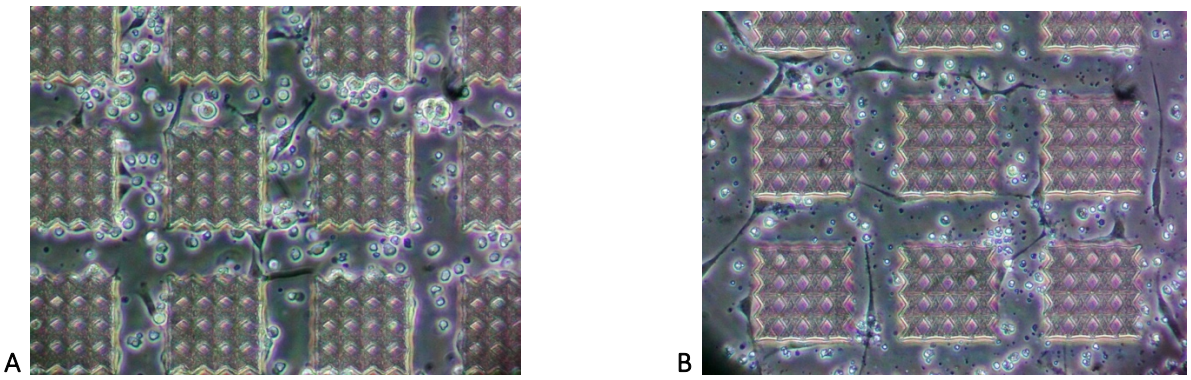

Fig. 5 Example images of the two cell lines used on the structures **A** Affected NPCs (AD2) on the large-scale structure **B** Healthy NPCs (LL90) on the large-scale structure

As next step we wanted to investigate whether the structures were in fact big enough for the cells to enter inside. While the size of the pores designed for the small structure ranged from 5.6 – 131 μm^2 and for the large one from 19 – 387 μm^2, the resin used for their manufacture can shrink after development. To evaluate cell interaction with the structures, we performed phalloidin and DAPI staining and used confocal microscopy to reconstruct a z-stack of the structures across their depth (Fig. 6).

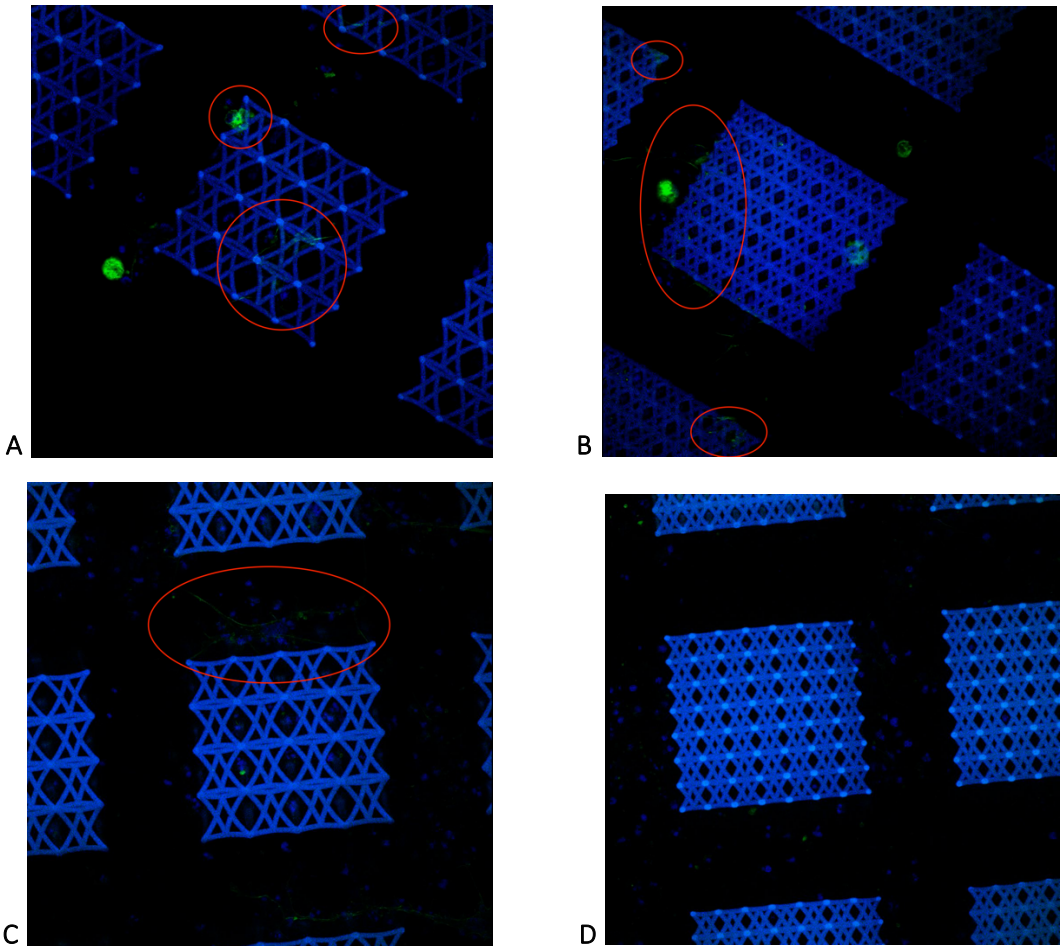

Fig. 6 Representative confocal microscopy pictures (63X) **A** Affected NPCs (AD2) on the large-scale structure **B** Affected NPCs (AD2) on the small-scale structure **C** Healthy NPCs (LL90) on the large-scale structure **D** Healthy NPCs (LL90) on the small-scale structure. Red circles showing cells interacting with the scaffolds.

The preliminary image analysis suggests that it was easier for the cells to infiltrate the large-scale structures, as we have noticed more interactions and cells going deeper inside the structures. We have also seen that the affected cells were interacting more with the structures, however the pictures of the healthy cells showed a lot of stained nuclei, which could signal increased cell death and could result in little interactions observed there.

Hydrogels (Stiffness)

In order to investigate the differences in cellular morphology depending on different scaffold stiffness we have used hydrogels provided by our collaborators. We first compared different bases: gelatin and alginate, however alginate proved to be not stable enough as it was

disintegrated when the medium was removed. After two weeks of culture, we have performed staining with phalloidin and DAPI to investigate the morphology of the cells (see Fig. 7).

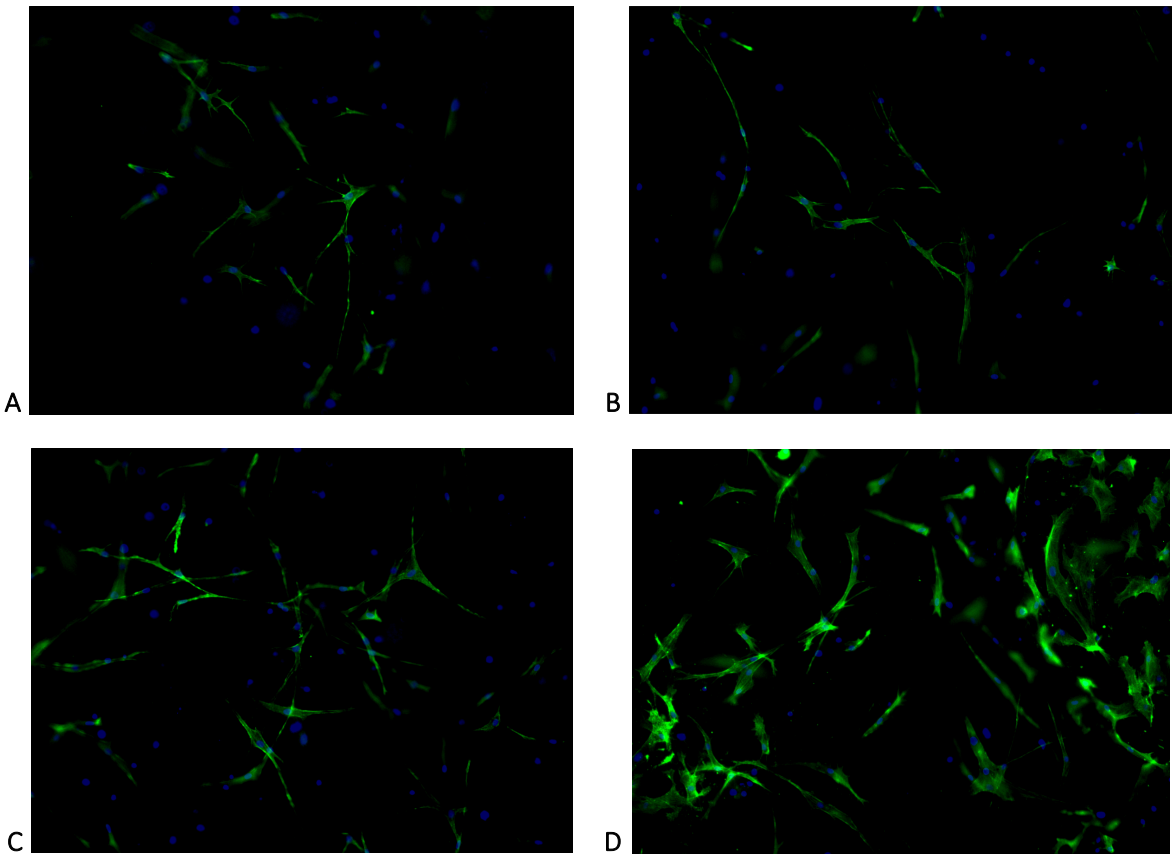

Fig. 7 Phalloidin and DAPI stainings of NPCs in the gelatin hydrogels of varying stiffnesses **A** 0.5 kPa **B** 2 kPa **C** 4 kPa and **D** 8 kPa

As visible in the pictures, there are clear differences in regard to cell number and their morphology according to the hydrogel stiffness. It seems that the stiffer gel promoted higher proliferation, while the morphology of the cells was more elongated in the softer one. We have also noticed more nuclei in the softer gels, which could be an indication of incomplete or inefficient phalloidin staining.

DISCUSSION

Here we presented ways in which we can further investigate three different aspects of the EMC influence on neural stem cell proliferation and differentiation and compare the differences between healthy and AD-derived cells. First, we have performed decellularization on various porcine brain regions and identified ways in which our procedure can be improved. Second, we seeded NPCs on 3D structures of two different scales and identified the optimal design for

future studies. Finally, we have observed different morphologies of NPCs seeded in hydrogels of different stiffnesses.

Composition

We have decellularized 11 different areas of porcine brain in order to optimize our procedure. We have used porcine tissue since it is a good model of the human matrix (Simsa et al., 2021). It was previously reported that cells were able to attach and grow on decellularized porcine ECM derived from either cortex, cerebellum or the remaining regions (Reginensi et al., 2020). Moreover, iPSCs have been previously shown to successfully differentiate on porcine brain-derived ECM-based coating into neurons (DeQuach et al., 2011). While cells from neural crest have been shown to respond differently to CNS and non-CNS scaffolds in terms of their mobility and differentiation (Crapo et al., 2012), our goal was to model not only CNS generally but also specific brain regions.

Cells adhere to the ECM through receptors such as integrins, influencing their shape and motility, as well as plasticity and synapse formation (Pavlov et al., 2004). The ECM can also bind growth factors and interact with cell receptors playing a role in the post-translational modifications and other important processes (Frantz et al., 2010). Since different brain regions have different matrix compositions, our ECM could provide specific structural cues and neurotrophic factors for the cells. Therefore, including the ECM in the proliferation and differentiation process can be of big importance, especially since stem cells are heavily influenced by the signaling of the ECM molecules (Hoshiba et al., 2016). The ECM could also help us see how differently the AD and healthy patients-derived NPCs interact with their environment.

The method of decellularization has huge impact on the quality of the final product (Fernández-Pérez & Ahearne, 2019), with the most difficult task being keeping the balance between removing cells and retaining the characteristic proteins and composition of the ECM. Here we have decellularized the porcine brain tissue through initial incubations on agitation with Triton X-100 (a non-ionic detergent) which disrupted the interactions between lipids and later with sodium deoxycholate (an ionic detergent) which is better for long washes as it can preserve the scaffolds better. Alternative detergents could be used, as well as physical (e.g. freeze-thawing

or including centrifugation) or biological (through enzymes such as trypsin or pepsin) methods. The various other decellularizations methods and detergents used across experimental designs are reviewed elsewhere (Buckenmeyer, Meder, Prest, & Brown, 2020).

Brain is an especially hard organ to decellularize as it falls apart quite easily (DeQuach et al., 2011), and while we have observed that cutting the tissue into small pieces was beneficial for the duration and the quality of the final ECM, it was also suggested to increase the overall tissue loss, up to even 98,7% (Simsa et al., 2021). However, using our method, we have retained between 4,24% and 14,23% of the primary weight after decellularization. Still, an even shorter protocol than ours might be beneficial since it would decrease the risk of losing a lot of the ECM proteins. Performing an additional protein content measurement will allow for a more detailed analysis. Moreover, the duration of our procedure (up to 26h spread over several days with several washes per day), could increase contamination risk so it would be recommended to sterilize the matrix before using it further or add penicillin/streptomycin mix into the incubation steps, especially since we have not been working in sterile conditions.

We have also quantified the DNA content before and after the decellularization to assess the efficacy of the procedure and the potential immunogenicity of our samples. The three criteria which are usually used in the literature are: absence of nuclei in histological DAPI stainings, lack of DNA fragments longer than 200 bp and less than 50 ng/mg of DNA per lyophilized ECM, with the latter one being most commonly used (Crapo, Gilbert, & Badylak, 2011). It is worth noting here that these are not definite criteria, with some authors using e.g. ng/mg of wet tissue (Simsa et al., 2021), and some also reporting % of original DNA content removed, with around 90% or 95% being the often reported value (DeQuach et al., 2011; Reginensi et al., 2020). While we have observed a huge decrease in the DNA content (2.18 ng/mg from 123.3 ng/mg of wet tissue) it does not meet the criteria of <50 ng/mg, since this value applies to lyophilized tissue. When we calculate our results with reference to the lyophilized weight, it is equal to 801.6 ng/mg. However, since we have not performed lyophilization on the pre-decellularized fragment, we cannot clearly compare or use this value. Despite that, since we have removed 98,23% of the original DNA content, the matrix should not induce an adverse immune reaction. Furthermore, since we have only quantified one fragment (which was decellularized as the first one), this analysis should be repeated for a different brain region. For future decellularizations,

adding a step of washing with DNAse could prove useful since it can increase fragmentation of the DNA (Fernández-Pérez & Ahearne, 2019). Additionally, the detergents we used here were previously shown to not remove as much cellular content as other methods (DeQuach et al., 2011), so including a different one could help in purifying the final matrix.

3D Structures

Another important aspect of the microenvironment is its structure (Fernández-Pérez & Ahearne, 2019). Here we aimed to optimize the size and characteristics of 3D polymeric structures on which we seeded NPCs generated from AD patients and healthy controls. Based on confocal microscopy pictures we were able to see that the cells were able to infiltrate the large-scale structure easier than the small-scale ones. The healthy cells seemed to have higher cell death and lower proliferation rate, however they also showed more elongated morphology. The affected ones interacted more with the scaffolds, which could be a result of various characteristics, such as different set of surface proteins. This, together with the proliferation rate and viability after seeding, will require further investigation.

The ECM defines the physical properties of the extracellular space by forming a complex meshwork which provides mechanical scaffold for interacting cells. In trying to mimic this structure, many aspects are important to consider such as pore shape, size and channel length, however the limiting factor is the size of a cell's nucleus which is much stiffer than cytoplasm, so while the cell can deform its shape to fit a given matrix, the nucleus cannot (Lammerding, 2011). The average size of the nucleus of NPCs has not yet been described so we used the average size of the SH-SY5Y cells' nuclei as a guiding value (George et al., 2018). The structures must also be resistant to biodegradation and not release toxic compounds even after long incubation times which are necessary for differentiation processes of NPCs. Aspects such as roughness and porosity are important for adhesion and proliferation, especially in the context of perfusion of oxygen and nutrients (Fan et al., 2019).

Microporous membranes have been tested before with neuron-like cells (George et al., 2018). It was shown that neurites can grow through the micro-channels which supported interactions between cells. Moreover, the pore size had a big influence on the cells – the area covered by neurons which migrated to the non-seeded side of the scaffold was proportional to the

diameter of its channels. Interestingly, when cells were non-confluent there was significant reduction in how much they penetrated the membrane through the pores. This could have also influenced the interaction rate in our experiment. In the following studies, it will be useful to increase the number of cells seeded, as well as to increase the pore size of the scaffolds.

Stiffness

ECM influences the cells not only through interactions with proteins and receptors, but also by determining physical properties of their environment, such as stiffness (Pavlov et al., 2004). To investigate its importance for NPCs, we have used two types of hydrogel with two different bases: alginate and gelatin. The latter proved to be more stable, and for future studies gelatin should be used. Alternatively, a technique often used is blending of the two gel substrates. A more extensive analysis of possible substrates is reviewed elsewhere (Fan et al., 2019). Between the four stiffnesses included in this experiment (0.5 kPa, 2 kPa, 4kPa, 8kPa), we have observed differences in the morphology of the NPCs, with the lowest values corresponding to AD, and the highest to tumorous cells which tend to be stiffer and also stiffen the ECM around them (Fiore et al., 2020). In stiffer gels the cells proliferated more, and in softer environment they had a more elongated body. This corroborates previous findings of greater neurite extension in softer, rather than stiffer hydrogels (Stukel & Willits, 2018). In softer gels we could also see more nuclei, which could mean either increased cell death or it could be that the permeabilization time during the phalloidin staining was too short so that not all the cells were fully visualized.

When cells have to anchor on a plastic dish, they encounter tension which is thousand times higher than that of their natural microenvironment in the body. Especially when compared with the brain, which is in general a very soft tissue (Discher, Mooney, & Zandstra, 2009). Moreover, in AD there is a further decrease of brain stiffness, with AD patients having median of 2.20 kPa, when compared to 2.37 kPa of healthy age-matched volunteers with no visible amyloid beta (Murphy et al., 2011). This reduction was not directly related to amyloid accumulation, but it could be connected to changes in the cytoarchitecture, or structural integrity as a result of ECM degradation. Significant reduction of stiffness was also found in hippocampus, which is a crucial brain area for memory and one of the earliest and most severely affected by AD plaques (Gerischer et al., 2018).

It is important to note here that these types of stiffness changes are not exclusive to AD, but occur in various other diseases, as well as in healthy aging. Even in nervous system development the way axons grow and find their paths is based not only on biochemical cues but also local stiffness (Koser et al., 2016). Interestingly, controlling substrate stiffness can have an effect on fate determination of stem cells, with neuronal lineage being preferred at 1 kPa and glial cell one being chosen at 10 kPa (Her et al., 2013). This, together with the fact that we can observe precocious differentiation of AD-derived NPCs (Amponsah et al., 2021) and reduced progenitor cell renewal (Meyer et al., 2019), suggests that by influencing the stiffness we could potentially influence stem cell fate determination and revert this disease phenotype. Including AD cells in the above described hydrogels of varying stiffnesses, and comparing their differentiation process and final markers of neuronal identity with that of healthy cells could help in answering these questions.

Conclusion

The ECM is a dynamic, constantly remodeled structure which includes both the physical scaffoldings and biochemical cues. It is crucial for the development of the NPCs and plays an important role in AD progression. We have shown here preliminary data on the interactions between NPCs and various aspects of the ECM, and delineated how the protocols and structures described above can be incorporated in further research. Eventually our goal is to compare the influence of the ECM from human brain regions on NPCs from AD and healthy individuals, with the obtained ECM used either as a coating or a hydrogel substrate. Changes in the ECM content can also influence the elasticity and structure of the tissue (Frantz et al., 2010), so incorporating different stiffnesses and the optimized 3D structures together with the decellularized matrix is necessary for accurate modelling of the brain microenvironment, in the diseased as well as healthy state.

APPENDIX 1 – TOXICITY OF FIBRILS ON NEURONAL CELLS

INTRODUCTION

Huntington's Disease (HD) is a heritable neurodegenerative disorder characterized by cognitive deficits, emotional impairments, chorea and dystonia (Walker, 2007). It is one of the CAG (cytosine-adenine-guanine) repeat diseases – in this case, the CAG triplet repeat in the first exon of the huntingtin protein (htt exon1) results in polyglutamine (polyQ) expansions at its N-terminus (Thakur et al., 2009). If this polyQ sequence expands above a certain threshold (around 36 repeats) there is a high risk of developing HD, with longer repeats being corelated with earlier onset (Andresen et al., 2007). These additional PolyQ peptides lead to protein misfolding, which then forms amyloid-like aggregates and eventually causes neuronal death.

While the intracellular inclusions containing protein aggregates are a well-known pathological characteristic of the disorder (Becher et al., 1998), no relationship between the visible aggregates and disease progression has been established (Poirier et al., 2002). In fact, the intracellular inclusions are thought to be protective, since they can cumulate the aggregated misfolded proteins in one place (Sahl, Weiss, Duim, Frydman, & Moerner, 2012). Importantly, the aggregates present are polymorphic meaning they can have different structures which in large part determine how toxic they will be for the cells (Sahl et al., 2012). Recently it has been suggested that the diffuse, fibrillar aggregates could be the most dangerous (Arrasate, Mitra, Schweitzer, Segal, & Finkbeiner, 2004), but the exact nature of these differences is not clear.

The different morphologies of fibril species and their specific toxic characteristics might be a result of different aggregation mechanisms which could dependent on the flanking sequences (Duennwald, Jagadish, Muchowski, & Lindquist, 2006). Specifically, the 17-amino-acid flanking sequence (HTT^{NT}) on its own forms a coil which does not aggregate, however the polyQ expansions cause it to unfold and facilitate aggregation (Thakur et al., 2009). The C-terminus, on the other hand, does not seem to be crucial for aggregation, and its polyproline flanking sequences seem to actually have an inhibitory effect (Isas, Langen, & Siemer, 2015). This conformational communication between the flanking regions and the PolyQ core means that modelling polyglutamine alone does not give a clear picture of the aggregation mechanics (Thakur et al., 2009).

Moreover, the way in which fibrils is prepared can influence its mechanics. Using a linker residue at the end of the PolyQ tail which inhibits its aggregation and is cleaved in order to start the process (Poirier et al., 2002) can influence the aggregation through altering the flanking domain. To take this into account, we have used short fibrils derived from the htt protein which incorporated the polyQ expansions as well as the alpha-helical N-terminal flanking segment (Lin et al., 2017). This was lacking from many fibrils prepared before, but it is thought to have a big influence on the size of the fibrils by clustering and becoming inaccessible to various PTMs (aggregation-modulating post-translational modifications), antibodies and chaperones which would otherwise modulate the aggregation processes (Isas et al., 2015).

Experimental Design

We have used HT22 (immortalized murine hippocampal neuronal cell line) and Luhmes cells (human dopaminergic neurons) as our models to determine the influence of fibrils on their viability and network formation. We have used fibrils from htt exon1 with a 44-residue polyQ. We have compared different durations of treatment, concentrations, sonication, and different types of preparation (FxA and Trypsin as enzymes cleaving the protein).

METHODS

Fibrils

For this experiment we tested two types of amyloid-like fibrils which had a 44-residue poly-Q in the exon1 of the huntigtin protein (HttEx1Q44), and which were generated as described previously (Lin et al., 2017). We have compared sonicated and non-sonicated fibrils, as well as two different types of preparation: with either FxA or trypsin. Lastly, we have compared different concentrations: 2.5 µM and 5 µM for HT22 cells, and 5 µM, 15 µM and 25 µM for Luhmes.

Neural Toxicity Assay – HT22 Cells

Mouse hippocampal HT22 cells were seeded on a 96-well plate with the density of $7x10^3$ cells/well or $4x10^3$ cells/well. Cells were treated with 5 µM HttEx1Q44 fibrils for 24h, 48h or 72h. Cell viability was assessed with the MTT Assay. Briefly, 0.5 mg/ml of the MTT (Sigma, #M2128-5) was added to the samples and the plate was incubated for one hour at 37°. The medium was then removed and the plate was stored at -20°. Before reading, 100 µl of DMSO was added in each well and incubated at 37° for 1h at agitation. The plate was read using the

Gen5 Software (Biotek) and the wavelengths measured were 570 nm for the MTT and 630 nm for the background. For analysis we have subtracted the background values from the MTT and calculated these as % of control.

Neural Network Integrity – Luhmes Cells

MEDIA AND REAGENTS. Lund human mesencephalic cells (LUHMES) were differentiated to dopaminergic neurons before the treatments as described before (Dolga et al., 2014; Lotharius et al., 2002). Proliferation medium was prepared with Advanced DMEM/F12, supplemented with 200 mM L-Glutamine (Gibco, #25030-024), 100x N2 Supplement, 100 µg/ml FGF and 100x penicillin/streptomycin solution. Differentiation medium was prepared with the same base medium supplemented with 200 mM L-Glutamine, 100x N2, 100 mM db-cAMP, 1 mg/ml tetracycline (Sigma, #T-7660) and 20 µg/ml GDNF. All NuclonTM flasks and plates were coated with 1 mg/ml poly-l-ornithine (Sigma, #P-3655) and 1 mg/ml fibronectin (Sigma, #F-1141) in H_20 and incubated for 3 hours, then stored at 3° until used. Cells were passed every other day with a 1:5 solution of trypsin (ThermoFisher, #25300062) in PBS.

LIVE CELL IMAGING. The cells were seeded at a density of $50x10^3$ cells/well in pre-coated 48-well Nuclon TM plate. After 6 days of differentiation the cells were treated with 5 µM of fibrils for 24h. They were then stained with Calcein-AM (Sigma, #C1359) and Hoestch (Invitrogen, #H3570) for live cell imaging. The pictures were taken with the Zeiss Cell Discoverer 7 Microscope and analyzed with the Fiji Macro Plug-In NeurphologyJ Interactive, with neurite area as the dependent variable (Ho et al., 2011).

STAINING. Before treatment the cells were pre-differentiated for 48h in the flask, then trypsynized and seeded at a density of $52x10^3$ cells/well in pre-coated 48-well NuclonTM plates. After 6 days of differentiation, HttEx1Q44 fibrils at two different concentrations (5 µM and 2.5 µM) was added. After 24h the cells were washed three times with PBS and fixed with 4% PFA solution for 15 minutes at RT. Cells were then again rinsed three times with PBS and kept at 3°. The cells were permeabilized by incubating in a solution of 1% Triton X-100 for 20 minutes at RT. They were then washed 3 times in PBS and incubated with Alexa Fluor 488 Phalloidin (1:40) and DAPI (1 µg/ml) for 1h at RT in the dark. Images were taken with the Zeiss Cell Discoverer 7

Microscope and analyzed with Fiji Macro Plug-In NeurphologyJ Interactive, with neurite area as the dependent variable (Ho et al., 2011).

Statistical Analysis

Statistical analyses were performed with GraphPad Prism Version 9.0 for Macintosh (GraphPad Software, San Diego, California, USA) using one-way ANOVA followed by Tukey's post-hoc test. Statistical significance was assumed at $p \leq 0.05$. All data are expressed as mean ± SD.

RESULTS

Neural Toxicity Assay - HT22 Cells

We have treated HT22 cells with fibrils to investigate its influence on their viability with the colorimetric MTT assay. First, we seeded the cells with the density of $7*10^3$ cells/well and we have seen no significant difference across most conditions (Fig. S1). The highest fibrils concentration seemed to cause a decrease in viability when compared to 15 µM, however this was mostly caused by unexpectedly high values of this condition (up to 120%), and importantly the 25 µM value was not significantly different than the control.

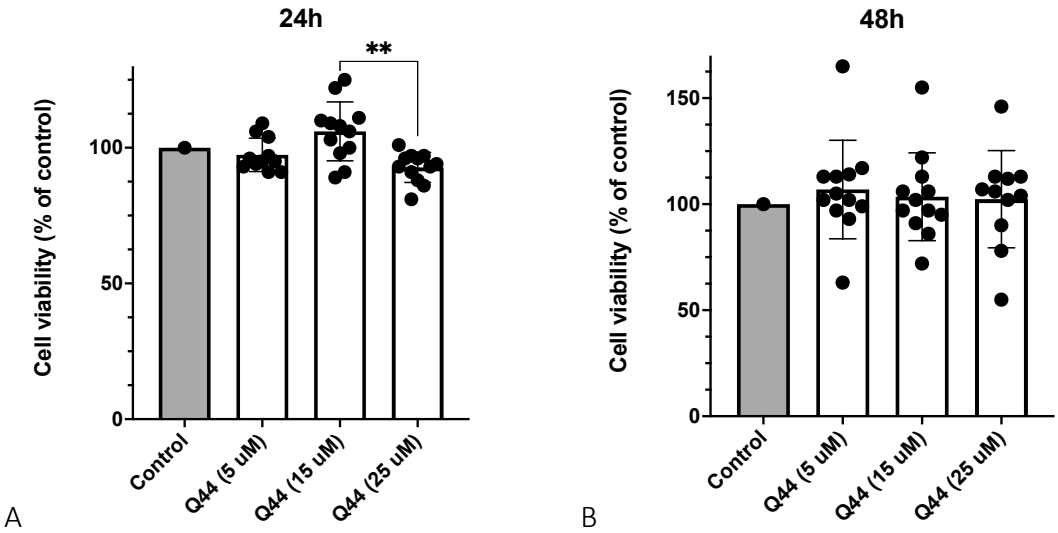

Fig. S1 Neural toxicity assay. Mouse hippocampal HT22 cells were treated with varying concentrations of HttEx1Q44 fibrils for 24h (**A**) and 48h (**B**). Data in the bar graph represents mean ± SD (one-way ANOVA with post-hoc Tukey; * $p \leq 0.05$; ** $p \leq 0.01$; n=1 with 10-12 technical replicates for each treatment)

Since in the first experiment the cells were very confluent, we hypothesized this could have led to no observable effect of fibrils and we have repeated the experiment with a smaller seeding density of $4*10^3$ cells/well. We have also used sonicated fibrils, to investigate whether

fragmenting it could make it more efficient. Finally, we have compared two different enzymes cleaving the proteins: FxA and Trypsin, and used only the highest concentration of fibrils – 25 µM. We have seen no significant differences in the cell viability when using sonicated fibrils in either 48h or 72h conditions (Fig. S2A, S2B). With the non-sonicated one, at 48h the trypsinized fibrils decreased the viability more strongly than FxA and similar non-significant trend was observed at 72h (Fig. S2C, S2D). We have therefore decided to continue with the non-sonicated fibrils created with trypsin for our final experiment.

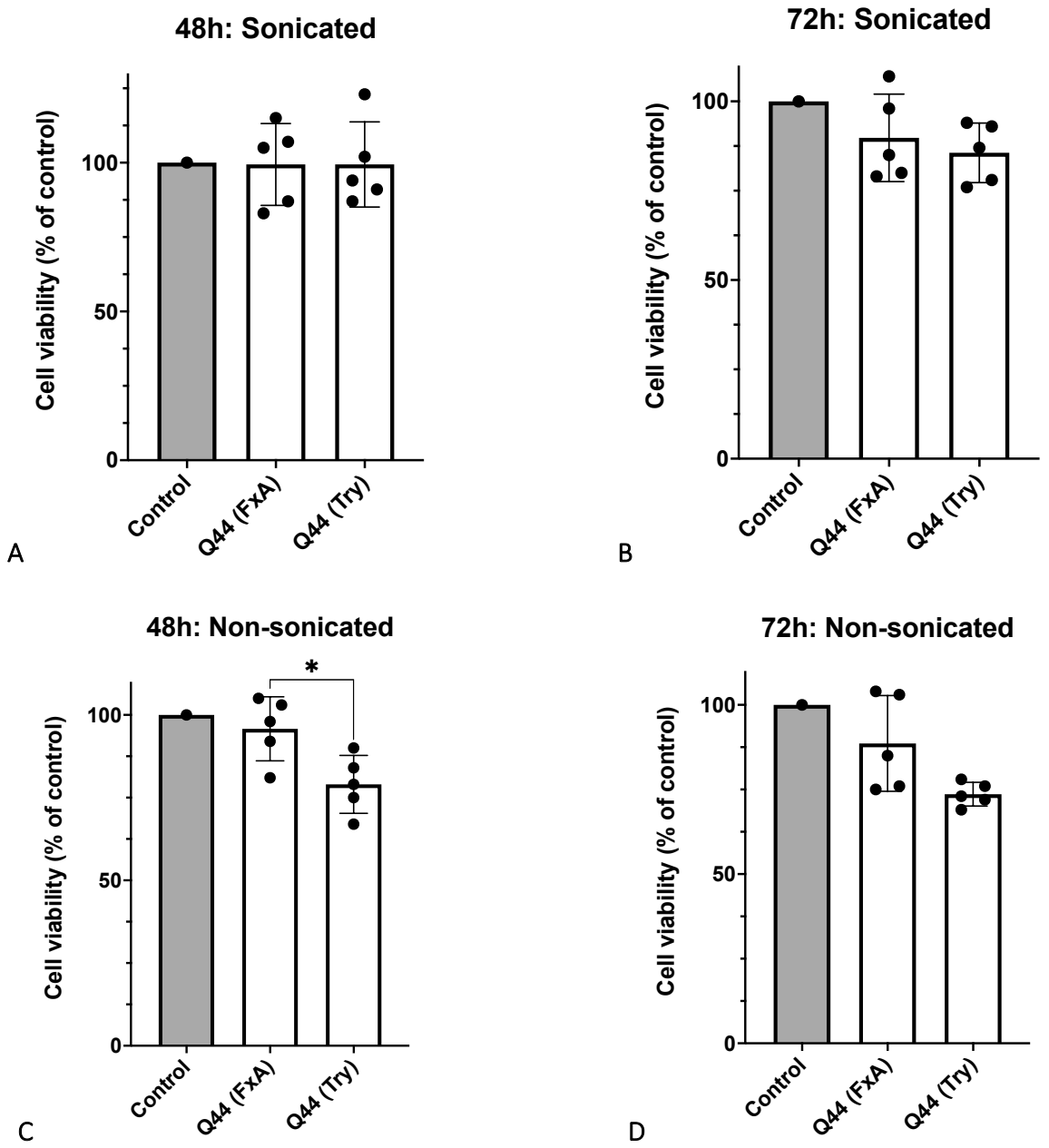

Fig. S2 Neural toxicity assay. Mouse hippocampal HT22 cells were treated for 48h and 72h with sonicated (**A, B**) or non-sonicated (**C, D**) HttEx1Q44 fibrils prepared either with trypsin or FxA. Data in the bar graph represents mean ± SD (one-way ANOVA with post-hoc Tukey; * $p \leq 0.05$; n=1 with 5 technical replicates for each treatment)

In the last experiment we have seen a clear effect of fibrils on the cell viability, both with 48h and 72h of treatment (see Fig. S3). Both concentrations used significantly decreased cell viability as compared with control (at 48h: 80% for 5 µM and 48% for 25 µM; at 72h: 41% for 5 µM and 14% for 25 µM). Moreover, the higher concentration had a significantly stronger effect than the lower, and both effects were more pronounced at 72h as compared with 48h.

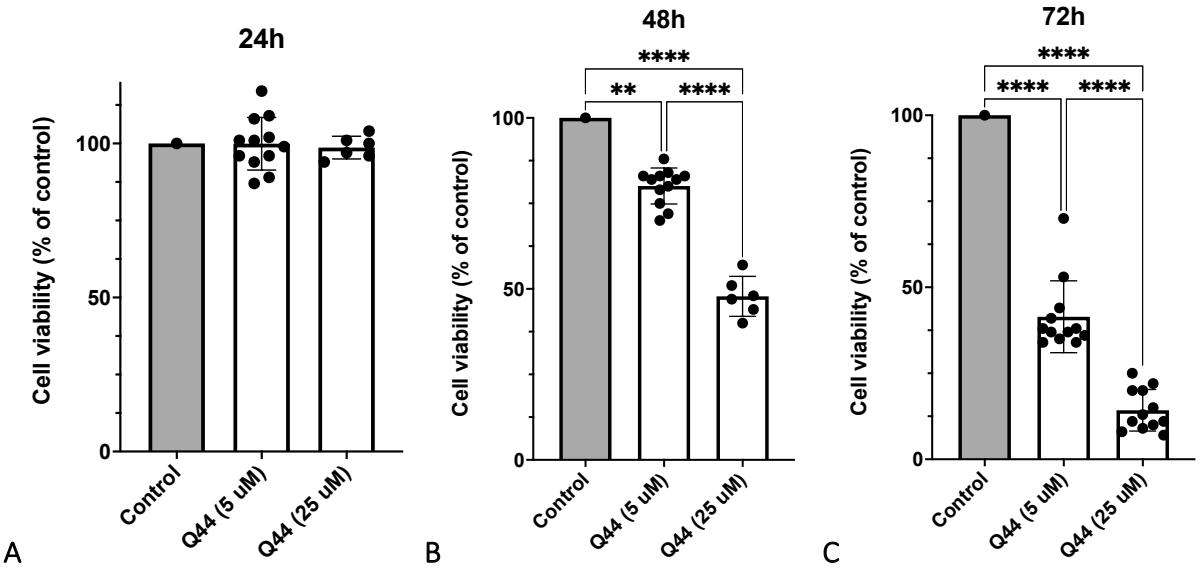

Fig. S3 Neural toxicity assay. Data in the bar graph represents mean ± SD (one-way ANOVA with post-hoc Tukey; ** $p \leq 0.05$; ** $p \leq 0.01$; *** $p \leq 0.001$; **** $p \leq 0.0001$; n=1 with 6-12 technical replicates for each treatment)

Neuronal network integrity - Luhmes Cells

To further investigate the influence of fibrils on neuronal cells, we have used a human dopaminergic Luhmes cell line. In order to evaluate their neuronal integrity, we have first performed a live cell imaging after 24h of treating Luhmes with 5 µM of non-sonicated fibrils prepared either with FxA or trypsin. We have seen no significant differences in either condition, and while there was a trend for decreased neurite area after treatment, more replicates are needed to conclude this (Fig. S4A). We have also performed a phalloidin staining on cells which were pre-differentiated for 48h and then treated with two different concentrations of non-sonicated fibrils for 24h (Fig. S4B). This treatment did not induce any significant changes in the neurite area of the cells.

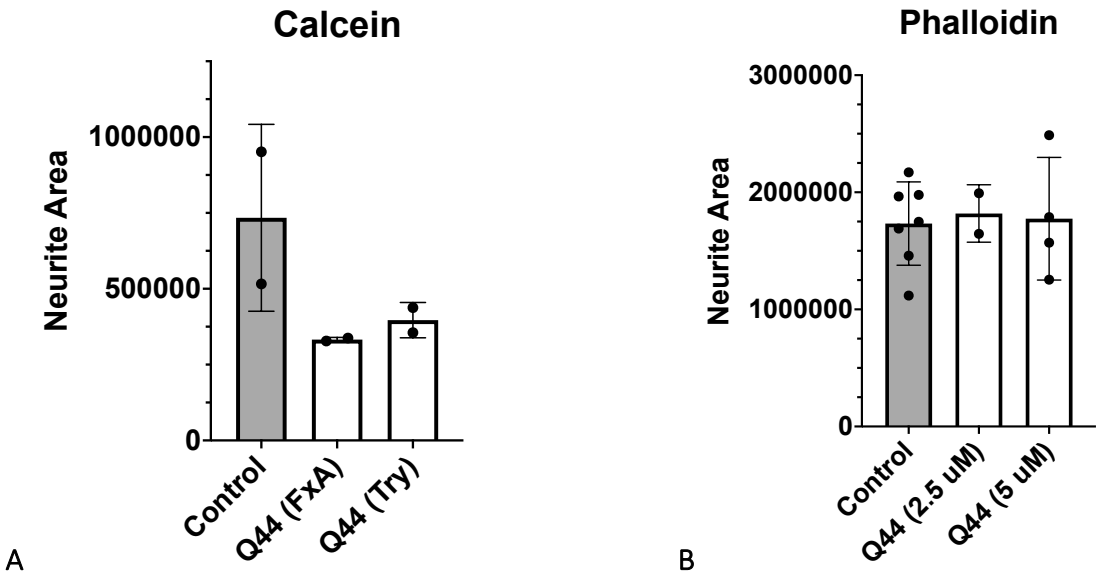

Fig. S4 Fibrils on human LUHMES dopaminergic neurons **A** Live cell imaging: cells differentiated for 6 days then treated for 24h with 5 uM of non-sonicated HttEx1Q44 **B** Phalloidin imaging: cells pre-differentiated for 48h then treated for 24h with two different concentrations of non-sonicated HttEx1Q44. Data in the bar graph represents mean ± SD (one-way ANOVA with post-hoc Tukey; * $p \leq 0.05$; n=1 with 2-7 technical replicates for each treatment)

DISCUSSION

In our experiments we have found that non-sonicated fibrils had more of an effect on murine hippocampal neurons that sonicated one and that using trypsin as the cleaving enzyme seemed to be more effective than using FxA, both after 48h and 72h of treatment. Moreover, we have found that the effect was time-dependent, being more pronounced with longer treatment, and that 25 µM concentrations decreased the viability of the cells more strongly than the 5 µM. In a previous study (Lin et al., 2017), the murine neurons were found to be significantly affected already at 24h and with the concentration of only 5 µM, possibly due to using sonicated fibrils which in our case did not seem to increase the toxicity. We have also performed network integrity assays on dopaminergic human neurons treated with fibrils instead of cell viability one since it allows for more detailed analysis of not only death but also impairments in the network. While neither showed significant difference, the calcein staining suggested a decrease as a result of treatment with fibrils. However, the treatment time was equal to only 24h and we had only 2 replicates of the experimental conditions so to obtain reliable results this experiment will have to be repeated. For the phalloidin staining we did not see any difference, however the small number of replicates does not allow to draw any strong conclusions.

Recently, the ability of purified polyQ-expanded Htt peptides to mimic what happens in the actual disease has been questioned (Duim, Jiang, Shen, Frydman, & Moerner, 2014). The aggregates are highly complex in nature, and can be formed directly from monomers or through oligomeric intermediate. One of the aspects modulating the conformation are the flanking amino acids (Legleiter et al., 2010). In fact, the synthetic polyQ without those domains show different aggregation kinetics, since the alpha-helix at the N-terminal crucially contributes to the stability of the fibrils (Lin et al., 2017). The proline-rich C-terminal helix is also important since it can decrease aggregation. Moreover, with long repeat parts of the flanking domains which are close to polyQ can become clustered so that antibodies which could potentially inhibit the aggregation processes cannot reach them anymore (Isas et al., 2015). The fibrils which we used here retained its flanking domains – most importantly, the alpha-helix at the HTT^{NT}, so it allows for a more accurate modeling of the disease (Lin et al., 2017).

The functional mechanisms through which fibrils exerts its toxic effects are not fully known, nevertheless one of the main pathways is thought to be through impairing the proteostasis network, maintained mainly by chaperones which are involved in clearance, folding and synthesis of proteins (Hartl, Bracher, & Hayer-Hartl, 2011). Accumulation of aggregates overwhelms the chaperones, which are not able to take care of other proteins, disrupting clearance and other crucial cellular processes. This cycle, in which not enough chaperones are available to clear out the increasing number of aggregates and to prevent further misfolding results in even faster aggregation and eventually contributes to the collapse of proteostasis network, cellular death and neurodegeneration.

Some specific chaperones have been identified as playing a role in Huntington's, for instance heat shock protein 40 (Hsp40) which is normally transporting proteins into the nucleus for degradation, but is depleted by polyQ and as a result misfolded proteins cannot undergo nuclear degradation and aggregate in the cells (Park et al., 2013). Heat shock protein 70 (Hsp70) is another chaperone which is sequestered by polyQ aggregates and as a consequence clathrin-mediated endocytosis (CME) is inhibited, for which Hsp70 is essential. This means that some crucial neural membrane receptors (e.g. AMPA) are not internalized anymore, and downstream effects include dysfunctions of LTP (Yu et al., 2014). Vesicle and receptor trafficking in neurons

(both pre- and post-synaptic membranes) is especially dependent on CME, so its dysfunction can play a central role in neurodegenerative disorders (McMahon & Boucrot, 2011).

In general, many other chaperones and components of the proteostasis network are affected by the aggregates, such as ubiquitin which is also necessary for protein degradation processes (Park et al., 2013). Moreover, functional depletion levels of a given molecule are different for each process and change throughout development and with aging, which helps in explaining the phenotypic complexity of the disease. Apart from overwhelming the proteostasis network, polyQ tails can also "kidnap" other important proteins into the aggregates (Sakahira, Breuer, Hayer-Hartl, & Hartl, 2002). In fact, while bigger inclusions are not thought to correlate with the disease stadium and they could actually be protective by sequestering all the aggregates in one place, they can also include a lot of these "kidnapped" proteins, impair cell metabolism and result in necrosis (Ramdzan et al., 2017). Moreover, it is important to not forget the role aging plays in the development of Huntington's and the fact that with time various organelles work less efficiently, including mitochondria, which further burdens the proteostasis network (Soares, Reis, Pinho, Duchen, & Oliveira, 2019).

Conclusion

This study provides further evidence for the toxic effect of fibrils on neuronal cells and the importance of the HTT^{NT} in the aggregation process. We found that our fibrils had a profound effect on the murine hippocampal neurons, whereas the data with human dopaminergic cells, while promising, need more replications. The suggested functional mechanisms of fibrils-induced toxicity are likely to co-exist, synergistically increasing the neurodegeneration over time. Finally, the differences in the toxicity of different species seem to lay not in their size but in the way in which they are formed, and specifically in the structure of the flanking domains which carry different characteristics – it is therefore crucial to correctly understand the mechanisms behind formation of fibrils, in order to understand its functional consequences.

APPENDIX 2 – FATTY ACID OXIDATION IN AD-DERIVED iPSCs and NPCs

INTRODUCTION

An important feature of neurodegeneration is the disturbance of the bioenergetics in the brain, since energy becomes especially important when the normal functions are impaired. Findings of hypometabolism (decrease in cerebral blood flow and mean cerebral oxygen consumption) in cases of Alzheimer's Disease (AD) date back to the 80s (Frackwiak, Possilli, & Legg, 1981). Specifically, since most cells in the brain use sugar (mainly glucose) as their energy source (Berg, Tymoczko, & Stryer, 2002), glucose metabolism can be impaired by amyloid beta (Drzezga et al., 2003). However, while glucose is the brain's main fuel, it has been shown that fatty acid oxidation (FAO) also plays an important role, with astrocytes – cells responsible for the energy supply for the neurons, having a preference for fatty acids over glucose (Ebert, Haller, & Walton, 2003). Moreover, in AD there is a correlation between defective FAO, hippocampal neurodegeneration and even cognitive outcomes such as memory loss (Konttinen et al., 2019).

Cell metabolism is also a crucial aspect in the renewal of stem cells, and fatty acid metabolism specifically plays a role in stem cell fate decisions (Ito & Suda, 2014). Improving FAO is linked to improved neurogenesis and inhibiting it in NPCs with etomoxir led to decreased consumption of oxygen, as well as downregulated proliferation (Stoll et al., 2015). This inhibitor works through blocking carnitine palmitoyltransferase 1 (Cpt1), a rate-limiting enzyme which assists in transferring the fatty acids to the mitochondria and therefore allows for beta oxidation to occur (Jernberg, Bowman, Wolfgang, & Scafidi, 2017). During proliferation of the NPCs, which is crucial for hippocampal neurogenesis and cognitive processes, there seems to be a metabolic change in the rate of the FAO which regulates the balance between the proliferative and quiescent states (Knobloch et al., 2017). If the cells are quiescent, there is an upregulation of Cpt1-dependent FAO, and if it is decreased they proliferate more – manipulating the FAO was also enough to influence their proliferation rate.

Since FAO is important for neurogenesis and proliferation, the molecules regulating this process should also play an important role in the NPCs. Fatty acid binding proteins (Fabps) are lipid trafficking proteins, responsible for intracellular transport of fatty acids (Furuhashi & Hotamisligil, 2008). They have different affinities for different types of FAs, and the three types expressed in the brain are: Fabp3 (heart-type Fabp; H-Fabp), Fabp5 (epidermal-type Fabp; E-

Fabp) and Fabp7 (brain-type Fabp, B-Fabp) (Moullé, Cansell, Luquet, & Cruciani-Guglielmacci, 2012). During postnatal hippocampal neurogenesis Fabp5 and Fabp7 are crucial for proliferation and survival of the NPCs, which show high expression levels for both proteins, but each of them has a differential role (Matsumata et al., 2012). Fabp3 on the other hand has been proposed as a marker for AD (Sepe, Chiasserini, & Parnetti, 2018).

Experimental Design

Here we investigated the differences in expression levels of genes encoding the proteins described above (Cpt1a – isoform mainly expressed in astrocytes, Fabp3, Fabp5 and Fab7) between NPCs and iPSCs derived from AD patients with PSEN1ΔE9 mutation, and isogenic control lines in which the mutation was corrected using the CRISPR/Cas9 technique (Oksanen, Petersen, Naumenko, Puttonen, Lehtonen, Gubert Olivé, et al., 2017). We have performed real-time quantitative PCR to uncover the differences between the healthy and affected end-stage NPCs, as well as between the differentiation processes from iPSCs to NPCs.

METHODS

RNA was collected from NPCs and iPSCs according to the NucleoSpin protocol (Macherey-Nagel, #740955.50). The mRNA content was then determined using a NanoDrop Spectrophotometer (ND-1000). For PCR analysis, 1 µg of RNA was reverse transcribed to cDNA. First, RNA in RNAse-free water was added to 10 mM of dNTP's (Promega; #U151A) and 0.5 µg/µl of random primers (Promega; #C118A). Samples were then put on 70° for 5 min in a Doppio Thermal Cycler. For the final step of the cDNA synthesis, we added 1 µl of RNasin Ribonuclease Inhibitor (Promega; #N251B), 1 µl M-MLV Reverse Transcriptase (Promega; #M1708) and 5 µl of M-MLV 5X Reaction Buffer (Promega, #M531A) per sample. The last thermal cycle was as follows: 10 min at 25°C, 50 min at 37°C and 15 min at 70°C. The samples were then stored at 4°C. The AD4 Cl 1.6 and its isogenic control AD4 Cl 1.6.12.10 were used for the gene expression analysis (Table S1). For each biological replicate, 3 technical replicates were performed.

Table S1. Cell lines and passages used for cDNA synthesis.

AD4 1.6	AD4 1.6.12.10
p. 3.3	p. 3.4
p. 3.4	p. 3.5
p. 3.5	p. 3.5
p. 3.6	
p. 3.8	

Real time PCR amplification was then carried out on a 384-well plate in the QuantStudio 7 Flex Real-Time PCR System (ThermoFisher, #4485701). The genes of interest (GOI) analyzed were Fabp3, Fabp5, Fabp7 and Cpt1a. Reference genes used for normalizing the levels of mRNA of interest were HPRT, HMBS and RPL13a. Primers of all the genes are described below (Table S2). To each well 1 µl of cDNA was added and then centrifuged at 1000 rpm for 1 min. Then 9 µl of a pre-prepared mix was added to each sample, which consisted of 0.1 µl of appropriate forward and reverse primer each, 3.8 µl of RNAse-free water and 5 µl of SYBR Green (Roche; #04913914001). The plate was then sealed and centrifuged again with the same parameters as before. The reaction settings were: 1 cycle of 95°C for 20 seconds; 45 cycles of: 95°C for 1 second, 60°C for 20 seconds. After the reaction, the DNA product dissociation curve was determined, the temperature was raised to 95°C for 15 sec for DNA denaturation, the temperature was maintained at 60°C for 1min, followed by a gradual rise in temperature to 95°C. For the management of the thermal cycler and data collection, the QuantStudio Real-TimePCR Software (AppliedBiosystems) software was used. The results were analyzed as described before, as relative values to the control samples (Pfaffl, 2001).

Table S2. Primers' sequences

Primer	Sequence
Cpt1a_F_human	ATG CGC TAC TCC CTG AAA GTG
Cpt1a_R_human	GTG GCA CGA CTC ATC TTG C
Fabp3_F_human	TCA CCT GCA GAA ATG GGA CG
Fabp3_R_human	GCA GTC AGG TCA TGC CTC TT
Fabp5_F_human	TAG CTT TGC GAA AAA TGG GCG
Fabp5_R_human	TTC TGC CAT CAG CTG TGG TTT
Fabp7_F_human	GCA CAT TCA AGA ACA CGG AGA
Fabp7_R_human	CAC ATC ACC AAA AGT AAG GGT CA
RPL13a_F	TCG TAC GCT GTG AAG GCA TC
RPL13a_R	GCT TTT TCT TGT CGT AGG GGG
hHPRT_F	TCA TTA TGC TGA GGA TTT GGA AAG
hHPRT_R	GGC CTC CCA TCT CCT TCA TC
hHMBS_F	TGG ACC TGG TTG TTC ACT CCT T
hHMBS_R	CAA CAG CAT CAT GAG GGT TTT C

Statistical Analysis

Statistical analysis was performed with Microsoft Excel and GraphPad Prism Version 9.0 for Macintosh (GraphPad Software, San Diego, California, USA) using one-way ANOVA followed by

Tukey's post-hoc test. Statistical significance was assumed at $p \leq 0.05$. All data are expressed as mean ± SD.

RESULTS

We have performed a qRT-PCR to investigate differences in the beta oxidation-related gene expression that occur during the differentiation process from iPSCs and NPCs between AD-derived and isogenic control cells, as well as within the NPCs themselves. During the process of differentiation (Fig. S5) there was a significant increase in the mRNA expression of three out of the four measured genes (Cpt1a, Fabp3 and Fabp5) in the isogenic pair, whereas no significant difference was measured in the AD pair.

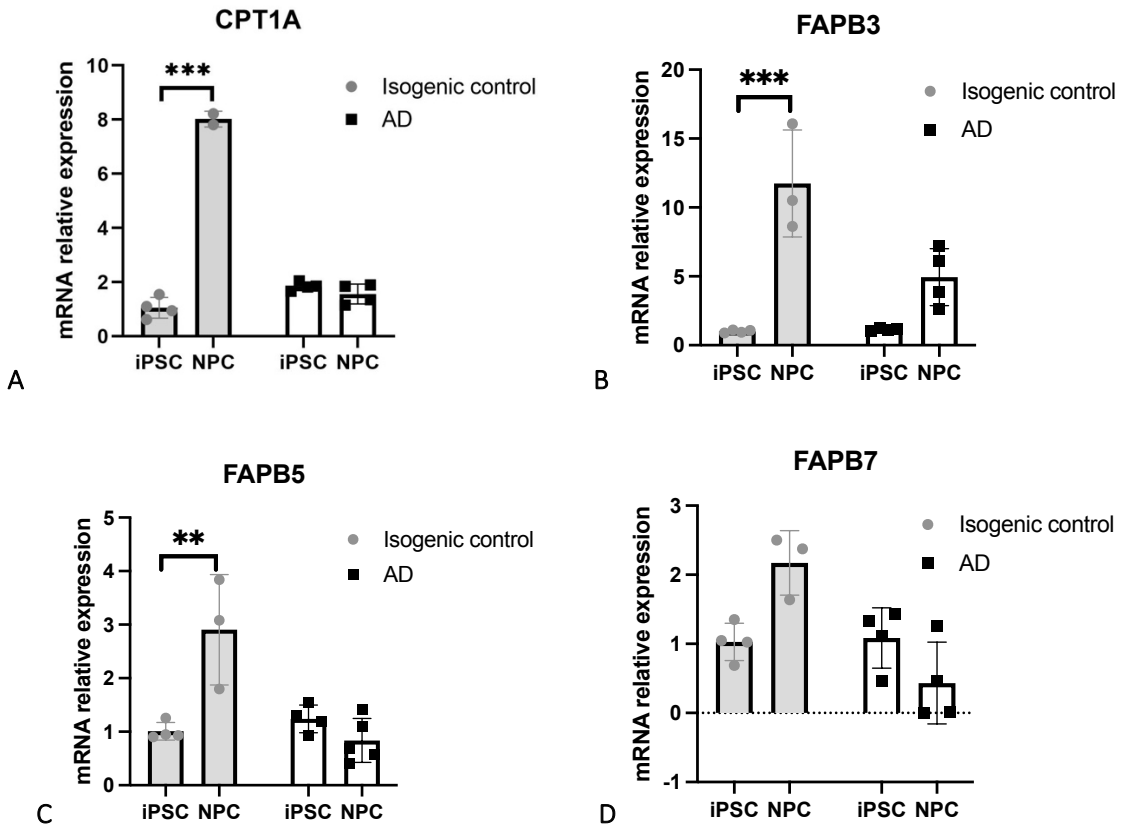

Fig. S5 Real-time quantitative PCR of the genes of interest: CPT1A (A), FAPB3 (B), FABP5 (C), FABP7 (D) in NPCs and iPSCs of affected and isogenic control cell lines. Data in the bar graph represents mean ± SD of the relative mRNA expression levels as compared to the average mRNA expression of housekeeping control genes normalized to iPSCs isogenic expression (n=3-5 for each comparison)

Within the NPCs comparison, the expression of all four genes was significantly lower in the AD-derived NPCs when compared to the isogenic controls (Fig. S6).

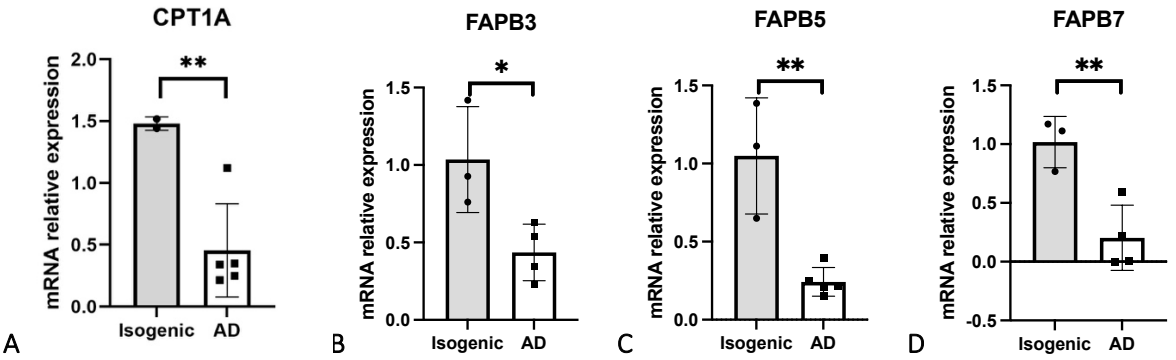

Fig. S6 Real-time quantitative PCR of the genes of interest: CPT1A (**A**), FAPB3 (**B**), FABP5 (**C**), FABP7 (**D**) in NPCs of affected and isogenic control cell lines. Data in the bar graph represents mean ± SD of the relative mRNA expression levels as compared to the average mRNA expression of housekeeping control genes normalized to NPCs isogenic expression (n=3-5 for each comparison)

DISCUSSION

We observed differences in the expression levels of genes encoding beta oxidation-related proteins between AD-derived and isogenic NPCs and iPSCs. Specifically, there was significant increase of the mRNA expression of Cpt1a, Fabp3 and Fabp5 between the iPSCs and NPCs of the isogenic controls, which was not evident in the affected cells, suggesting a dysfunction in the beta oxidation. The same trend was observed for Fabp7, but it was not statistically significant. Moreover, when comparing the expression levels of NPCs, all four genes were significantly less expressed in the AD-derived NPCs than in the isogenic controls.

Metabolic dysfunctions are a known phenomenon in patients with AD, mainly in the form of impaired glycolysis (Bigl, Apelt, Eschrich, & Schliebs, 2003), however there have also been findings of altered FAO (Ciavardelli et al., 2016). Generally, changes in lipid homeostasis are well-established in AD, since the most well-known risk factor is the APOEe4 (apolipoprotein E episol 4), which binds and transports lipids (Reitz, 2013). Lower levels of plasma acylcarnitines (ACC), involved in transport of long chain fatty acids and indicating changes in FAO, were found in individuals with AD and MCI, and could even be used to predict the conversion from MCI to AD at a later time point (Ciavardelli et al., 2016). In a mouse model of AD, an increased number of the very long chain fatty acids was found in the brain, which can accumulate and cause cognitive impairment (Bai et al., 2020). This study also found less polyunsaturated fatty acids (PUFAs) in the cerebral cortex of AD mice as compared with controls, which could play a protective role since they are correlated with decrease in oxidative stress, apoptosis and beta-amyloid levels.

PUFAs are important for brain development and correct functioning, however since they are lipophilic they require chaperones for transport, such as Fabps (Moullé et al., 2012). Each Fabp has preference for a different type of FA as its ligand (Sepe et al., 2018). Fabp3 increases in the brain with age, and is expressed, among others, in hippocampus and linked to neurite formation and synapse maturation (Owada, 2008). Fabp5 is present mostly around birth and its expression decreases with age. Interestingly, it is also enhanced in pathologies where neuronal regeneration occurs, and together with its timeline of expression it suggests a role in differentiation processes (Liu, Mita, Beaulieu, Gao, & Godbout, 2010). Fabp7 is barely present in adults, found mostly in the olfactory nerve, Purkinje cells and dentate gyrus (which is important for memory). However, it plays a big role in the embryonic brain, with high expression in radial glia, crucial for cell migration during brain development (Owada, 2008). The radial glia can also act as NPCs, with one study finding that all cells which expressed Fabp7 generated neurons at some stage (Anthony, Klein, Fishell, & Heintz, 2004).

Fabp3 levels were elevated in CSF of patients with AD when compared with controls (Rosén et al., 2011), and these levels could be used to distinguish between patients with AD and healthy controls, however significantly less effectively than with amyloid beta or tau levels (Sepe et al., 2018). Moreover, knockout of Fabp7 resulted in impaired proliferation and increased differentiation of NPCs during early cortical development (Owada, 2008), so this protein could contribute to neurogenesis through controlling the amount of NPCs and stem cells (Liu et al., 2010). Accordingly, another study found that this knockout attenuated neurogenesis in mice and specifically decreased astrocyte, NPC and neural stem cell number during brain development (Watanabe et al., 2007). Another study with mice found that knocking out either Fabp5, Fabp7 or both reduced the number of NPCs and their proliferation but enhanced differentiation in dentate gyrus, part of the hippocampal formation where most adult neurogenesis happens (Matsumata et al., 2012). Finally, a study involving monkeys with ischemia in their hippocampus found that while Fabp5 was non-existent in control brains (since its expression decreases with age), after injury it was significantly increased, as was Fabp7 to a smaller level, with no overall change to Fabp3. Seeing as Fabps have affinities for different FAs, these varied effects could be the result of depriving the cells of specific lipids which they bind to.

Cpt1 is a key enzyme in mitochondrial beta oxidation which converts long-chain fatty acyl-CoA to acylcarnitine and then transfers them across the mitochondrial membrane for degradation (Konttinen et al., 2019). Therefore, increased expression level of Cpt1 in our control cells suggests increased FAO since it limits the rate with which beta oxidation can occur. While the brain's main fuel is glucose, NPCs could have pathways specific to them which focus primarily on FAs, but which mechanism are not as easy to investigate due to their small number in the adult brain. A recent study found that NPCs are heavily influenced by changes in their metabolism – specifically, quiescent NPCs seem to have high Cpt1 expression, meaning higher functional FAO, and using malonyl-CoA, which inhibited Cpt1, induced proliferation of previously quiescent NPCs by regulation of the FAO levels (Knobloch et al., 2017). Oxidized fatty acids might therefore be an alternative energy source for the NPCs and the metabolic shift during the differentiation process could be impaired in AD and decrease neurogenesis.

Impairments in fatty acid oxidation have also been shown in astrocytes derived from iPSCs of AD patients with PSENΔE9 mutation (the same as our cells) and a synthetic peroxisome proliferator activated receptor delta agonist (GW0742) was shown to correct this impairment and counteracted fear conditioning memory impairments in a mouse model (Konttinen et al., 2019). Even though it did not change the amount of amyloid beta *per se*, it also increased neurogenesis and enhanced differentiation of NPCs, as well as prevented long-term potentiation deficits. The genes regulated by GW0742 were connected to cellular metabolism, among others Cpt1, which was increased, but it is important to notice that GW0742 affects also many other cellular pathways, having e.g. a huge antioxidant effect. However, since inhibiting Cpt1 with etomoxir blocked FAO in astrocytes, as well as counteracted the differentiation of the NPCs which was induced by GW0742, it is certainly a crucial player in this pathway. Importantly, since the cells used in our study were only at the iPSCs and NPCs stages, from which both astrocytes and neurons could develop, we are not able to determine at this stage which cell type retains these differences later on.

Conclusion

This study demonstrates clear differences in the expression of genes encoding FAO-related proteins between AD and isogenic controls. While here we used only one AD cell line, and in

the future this analysis should be repeated with others, it is coherent with reports of altered metabolism in AD patients specifically, as well as the role lipid metabolism plays in neurodegenerative disorders generally (Sepe et al., 2018). Fabps are essential tools for fatty acid transport and can therefore influence these metabolic pathways, while Cpt1a is a rate-limiting step in the mitochondrial beta oxidation. Inhibition of FAO can lead to increase in oxidative stress and that in turn can accelerate amyloid beta accumulation (Shi et al., 2016), so further investigation of the above-described molecules is necessary to elucidate the full mechanism behind AD.

REFERENCES

Amponsah, A. E., Guo, R., Kong, D., Feng, B., He, J., Zhang, W., . . . Liu, B. (2021). Patient-derived iPSCs, a reliable in vitro model for the investigation of Alzheimer's disease. *Reviews in the Neurosciences*.

Andresen, J. M., Gayán, J., Djoussé, L., Roberts, S., Brocklebank, D., Cherny, S. S., . . . Gusella, J. F. (2007). The relationship between CAG repeat length and age of onset differs for Huntington's disease patients with juvenile onset or adult onset. *Annals of human genetics, 71*(3), 295-301.

Anthony, T. E., Klein, C., Fishell, G., & Heintz, N. (2004). Radial glia serve as neuronal progenitors in all regions of the central nervous system. *Neuron, 41*(6), 881-890.

Antonova, O., Kochetkova, O., & Shlyapnikov, Y. (2021). ECM-Mimetic Nylon Nanofiber Scaffolds for Neurite Growth Guidance Neurites Growth on 60-nm Nylon Fibers. Nanomaterials 2021, 11, 516. In: s Note: MDPI stays neutral with regard to jurisdictional claims in published ….

Arrasate, M., Mitra, S., Schweitzer, E. S., Segal, M. R., & Finkbeiner, S. (2004). Inclusion body formation reduces levels of mutant huntingtin and the risk of neuronal death. *Nature, 431*(7010), 805-810.

Bai, Y.-R., Wang, Y.-Y., Meng, D.-L., Shi, Z.-L., Song, X.-F., Yang, Z.-Z., . . . Shi, R.-L. (2020). Alterations of fatty acid composition and metabolism in APP/PS1 transgenic mice. *Neuroscience Letters, 738*, 135401.

Barros, C. S., Franco, S. J., & Müller, U. (2011). Extracellular matrix: functions in the nervous system. *Cold Spring Harbor perspectives in biology, 3*(1), a005108.

Becher, M. W., Kotzuk, J. A., Sharp, A. H., Davies, S. W., Bates, G. P., Price, D. L., & Ross, C. A. (1998). Intranuclear Neuronal Inclusions in Huntington's Disease and Dentatorubral and Pallidoluysian Atrophy: Correlation between the Density of Inclusions andIT15CAG Triplet Repeat Length. *Neurobiology of Disease, 4*(6), 387-397.

Berg, J. M., Tymoczko, J. L., & Stryer, L. (2002). Biochemistry, ; W. H. *New York: Freeman and Company: New York*.

Bigl, M., Apelt, J., Eschrich, K., & Schliebs, R. (2003). Cortical glucose metabolism is altered in aged transgenic Tg2576 mice that demonstrate Alzheimer plaque pathology. *Journal of neural transmission, 110*(1), 77-94.

Braak, H., & Braak, E. (1991). Neuropathological stageing of Alzheimer-related changes. *Acta neuropathologica, 82*(4), 239-259.

Buckenmeyer, M. J., Meder, T. J., Prest, T. A., & Brown, B. N. (2020). Decellularization techniques and their applications for the repair and regeneration of the nervous system. *Methods, 171*, 41-61.

Ciavardelli, D., Piras, F., Consalvo, A., Rossi, C., Zucchelli, M., Di Ilio, C., . . . Sensi, S. L. (2016). Medium-chain plasma acylcarnitines, ketone levels, cognition, and gray matter volumes in healthy elderly, mildly cognitively impaired, or Alzheimer's disease subjects. *Neurobiology of Aging, 43*, 1-12.

Cortiella, J., Niles, J., Cantu, A., Brettler, A., Pham, A., Vargas, G., . . . Nichols, J. E. (2010). Influence of acellular natural lung matrix on murine embryonic stem cell differentiation and tissue formation. *Tissue Engineering Part A, 16*(8), 2565-2580.

Crapo, P. M., Gilbert, T. W., & Badylak, S. F. (2011). An overview of tissue and whole organ decellularization processes. *Biomaterials, 32*(12), 3233-3243.

Crapo, P. M., Medberry, C. J., Reing, J. E., Tottey, S., van der Merwe, Y., Jones, K. E., & Badylak, S. F. (2012). Biologic scaffolds composed of central nervous system extracellular matrix. *Biomaterials, 33*(13), 3539-3547.

DeQuach, J. A., Yuan, S. H., Goldstein, L. S., & Christman, K. L. (2011). Decellularized porcine brain matrix for cell culture and tissue engineering scaffolds. *Tissue Engineering Part A, 17*(21-22), 2583-2592.

Discher, D. E., Mooney, D. J., & Zandstra, P. W. (2009). Growth factors, matrices, and forces combine and control stem cells. *Science, 324*(5935), 1673-1677.

Dolga, A. M., de Andrade, A., Meissner, L., Knaus, H. G., Höllerhage, M., Christophersen, P., . . . Culmsee, C. (2014). Subcellular expression and neuroprotective effects of SK channels in human dopaminergic neurons. *Cell Death & Disease, 5*(1), e999-e999.

Drzezga, A., Lautenschlager, N., Siebner, H., Riemenschneider, M., Willoch, F., Minoshima, S., . . . Kurz, A. (2003). Cerebral metabolic changes accompanying conversion of mild cognitive impairment into Alzheimer's disease: a PET follow-up study. *European journal of nuclear medicine and molecular imaging, 30*(8), 1104-1113.

Duennwald, M. L., Jagadish, S., Muchowski, P. J., & Lindquist, S. (2006). Flanking sequences profoundly alter polyglutamine toxicity in yeast. *Proceedings of the National Academy of sciences, 103*(29), 11045-11050.

Duim, W. C., Jiang, Y., Shen, K., Frydman, J., & Moerner, W. (2014). Super-resolution fluorescence of huntingtin reveals growth of globular species into short fibers and coexistence of distinct aggregates. *ACS chemical biology, 9*(12), 2767-2778.

Ebert, D., Haller, R. G., & Walton, M. E. (2003). Energy contribution of octanoate to intact rat brain metabolism measured by 13C nuclear magnetic resonance spectroscopy. *Journal of Neuroscience, 23*(13), 5928-5935.

Fan, D., Staufer, U., & Accardo, A. (2019). Engineered 3D Polymer and Hydrogel Microenvironments for Cell Culture Applications. *Bioengineering (Basel, Switzerland), 6*(4).

Fernández-Pérez, J., & Ahearne, M. (2019). The impact of decellularization methods on extracellular matrix derived hydrogels. *Scientific reports, 9*(1), 1-12.

Fiore, V. F., Krajnc, M., Quiroz, F. G., Levorse, J., Pasolli, H. A., Shvartsman, S. Y., & Fuchs, E. (2020). Mechanics of a multilayer epithelium instruct tumour architecture and function. *Nature, 585*(7825), 433-439.

Frackwiak, R., Possilli, C., & Legg, N. (1981). Regional cerebral oxygen supply and utilization in dementia. *Brain, 104*, 753â.

Frantz, C., Stewart, K. M., & Weaver, V. M. (2010). The extracellular matrix at a glance. *Journal of cell science, 123*(24), 4195-4200.

Furuhashi, M., & Hotamisligil, G. S. (2008). Fatty acid-binding proteins: role in metabolic diseases and potential as drug targets. *Nature reviews Drug discovery, 7*(6), 489-503.

George, J. H., Nagel, D., Waller, S., Hill, E., Parri, H. R., Coleman, M. D., . . . Ye, H. (2018). A closer look at neuron interaction with track-etched microporous membranes. *Scientific reports, 8*(1), 1-11.

Gerischer, L. M., Fehlner, A., Köbe, T., Prehn, K., Antonenko, D., Grittner, U., . . . Flöel, A. (2018). Combining viscoelasticity, diffusivity and volume of the hippocampus for the diagnosis of Alzheimer's disease based on magnetic resonance imaging. *NeuroImage: Clinical, 18*, 485-493.

Granato, A. E., da Cruz, E. F., Rodrigues-Junior, D. M., Mosini, A. C., Ulrich, H., Rodrigues, B. V., . . . Porcionatto, M. (2020). A novel decellularization method to produce brain scaffolds. *Tissue and Cell, 67*, 101412.

Grimm, M. O. W., Rothhaar, T. L., & Hartmann, T. (2012). The role of APP proteolytic processing in lipid metabolism. *Experimental Brain Research, 217*(3), 365-375.

Gunhanlar, N., Shpak, G., van der Kroeg, M., Gouty-Colomer, L. A., Munshi, S. T., Lendemeijer, B., . . . Kushner, S. A. (2018). A simplified protocol for differentiation of electrophysiologically mature neuronal networks from human induced pluripotent stem cells. *Molecular Psychiatry, 23*(5), 1336-1344.

Hartl, F. U., Bracher, A., & Hayer-Hartl, M. (2011). Molecular chaperones in protein folding and proteostasis. *Nature, 475*(7356), 324-332.

Her, G. J., Wu, H.-C., Chen, M.-H., Chen, M.-Y., Chang, S.-C., & Wang, T.-W. (2013). Control of three-dimensional substrate stiffness to manipulate mesenchymal stem cell fate toward neuronal or glial lineages. *Acta Biomaterialia, 9*(2), 5170-5180.

Hiscox, L. V., Johnson, C. L., McGarry, M. D., Marshall, H., Ritchie, C. W., van Beek, E. J., . . . Starr, J. M. (2020). Mechanical property alterations across the cerebral cortex due to Alzheimer's disease. *Brain communications, 2*(1), fcz049.

Ho, S.-Y., Chao, C.-Y., Huang, H.-L., Chiu, T.-W., Charoenkwan, P., & Hwang, E. (2011). NeurphologyJ: An automatic neuronal morphology quantification method and its application in pharmacological discovery. *BMC Bioinformatics, 12*(1), 230.

Hoshiba, T., Chen, G., Endo, C., Maruyama, H., Wakui, M., Nemoto, E., . . . Tanaka, M. (2016). Decellularized Extracellular Matrix as an In Vitro Model to Study the Comprehensive Roles of the ECM in Stem Cell Differentiation. *Stem Cells International, 2016*, 6397820.

Isas, J. M., Langen, R., & Siemer, A. B. (2015). Solid-state nuclear magnetic resonance on the static and dynamic domains of huntingtin exon-1 fibrils. *Biochemistry, 54*(25), 3942-3949.

Ito, K., & Suda, T. (2014). Metabolic requirements for the maintenance of self-renewing stem cells. *Nature Reviews Molecular Cell Biology, 15*(4), 243-256.

Jernberg, J. N., Bowman, C. E., Wolfgang, M. J., & Scafidi, S. (2017). Developmental regulation and localization of carnitine palmitoyltransferases (CPT s) in rat brain. *Journal of neurochemistry, 142*(3), 407-419.

Knobloch, M., Pilz, G.-A., Ghesquière, B., Kovacs, W. J., Wegleiter, T., Moore, D. L., . . . Jessberger, S. (2017). A fatty acid oxidation-dependent metabolic shift regulates adult neural stem cell activity. *Cell reports, 20*(9), 2144-2155.

Konttinen, H., Gureviciene, I., Oksanen, M., Grubman, A., Loppi, S., Huuskonen, M. T., . . . Belaya, I. (2019). PPARβ/δ-agonist GW0742 ameliorates dysfunction in fatty acid oxidation in PSEN1ΔE9 astrocytes. *Glia, 67*(1), 146-159.

Koser, D. E., Thompson, A. J., Foster, S. K., Dwivedy, A., Pillai, E. K., Sheridan, G. K., . . . Franze, K. (2016). Mechanosensing is critical for axon growth in the developing brain. *Nature Neuroscience, 19*(12), 1592-1598.

Lammerding, J. (2011). Mechanics of the nucleus. *Comprehensive physiology, 1*(2), 783-807.

Legleiter, J., Mitchell, E., Lotz, G. P., Sapp, E., Ng, C., DiFiglia, M., . . . Muchowski, P. J. (2010). Mutant huntingtin fragments form oligomers in a polyglutamine length-dependent manner in vitro and in vivo. *Journal of Biological Chemistry, 285*(19), 14777-14790.

Lin, H.-K., Boatz, J. C., Krabbendam, I. E., Kodali, R., Hou, Z., Wetzel, R., . . . van der Wel, P. C. (2017). Fibril polymorphism affects immobilized non-amyloid flanking domains of huntingtin exon1 rather than its polyglutamine core. *Nature communications, 8*(1), 1-12.

Liu, R.-Z., Mita, R., Beaulieu, M., Gao, Z., & Godbout, R. (2010). Fatty acid binding proteins in brain development and disease. *International Journal of Developmental Biology, 54*(8-9), 1229-1239.

Lotharius, J., Barg, S., Wiekop, P., Lundberg, C., Raymon, H. K., & Brundin, P. (2002). Effect of mutant α-synuclein on dopamine homeostasis in a new human mesencephalic cell line. *Journal of Biological Chemistry, 277*(41), 38884-38894.

Matsumata, M., Sakayori, N., Maekawa, M., Owada, Y., Yoshikawa, T., & Osumi, N. (2012). The effects of Fabp7 and Fabp5 on postnatal hippocampal neurogenesis in the mouse. *Stem cells, 30*(7), 1532-1543.

McCoy, M. K., & Tansey, M. G. (2008). TNF signaling inhibition in the CNS: implications for normal brain function and neurodegenerative disease. *Journal of neuroinflammation, 5*(1), 1-13.

McMahon, H. T., & Boucrot, E. (2011). Molecular mechanism and physiological functions of clathrin-mediated endocytosis. *Nature Reviews Molecular Cell Biology, 12*(8), 517-533.

Meyer, K., Feldman, H. M., Lu, T., Drake, D., Lim, E. T., Ling, K.-H., . . . Lin, Y.-T. (2019). REST and neural gene network dysregulation in iPSC models of Alzheimer's disease. *Cell reports, 26*(5), 1112-1127. e1119.

Moullé, V. S., Cansell, C., Luquet, S., & Cruciani-Guglielmacci, C. (2012). The multiple roles of fatty acid handling proteins in brain. *Frontiers in physiology, 3*, 385.

Murphy, M. C., Huston III, J., Jack Jr, C. R., Glaser, K. J., Manduca, A., Felmlee, J. P., & Ehman, R. L. (2011). Decreased brain stiffness in Alzheimer's disease determined by magnetic resonance elastography. *Journal of magnetic resonance imaging, 34*(3), 494-498.

Oksanen, M., Petersen, A. J., Naumenko, N., Puttonen, K., Lehtonen, Š., Gubert Olivé, M., . . . Koistinaho, J. (2017). PSEN1 Mutant iPSC-Derived Model Reveals Severe Astrocyte Pathology in Alzheimer's Disease. *Stem Cell Reports, 9*(6), 1885-1897.

Oksanen, M., Petersen, A. J., Naumenko, N., Puttonen, K., Lehtonen, Š., Olivé, M. G., . . . Viitanen, M. (2017). PSEN1 mutant iPSC-derived model reveals severe astrocyte pathology in Alzheimer's disease. *Stem Cell Reports, 9*(6), 1885-1897.

Onesto, V., Accardo, A., Vieu, C., & Gentile, F. (2020). Small-world networks of neuroblastoma cells cultured in three-dimensional polymeric scaffolds featuring multi-scale roughness. *Neural regeneration research, 15*(4), 759.

Owada, Y. (2008). Fatty acid binding protein: localization and functional significance in the brain. *The Tohoku journal of experimental medicine, 214*(3), 213-220.

Park, S.-H., Kukushkin, Y., Gupta, R., Chen, T., Konagai, A., Hipp, M. S., . . . Hartl, F. U. (2013). PolyQ proteins interfere with nuclear degradation of cytosolic proteins by sequestering the Sis1p chaperone. *Cell, 154*(1), 134-145.

Pavlov, I., Lauri, S., Taira, T., & Rauvala, H. (2004). The role of ECM molecules in activity-dependent synaptic development and plasticity. *Birth Defects Research Part C: Embryo Today: Reviews, 72*(1), 12-24.

Pfaffl, M. W. (2001). A new mathematical model for relative quantification in real-time RT–PCR. *Nucleic Acids Research, 29*(9), e45-e45. doi:10.1093/nar/29.9.e45

Poirier, M. A., Li, H., Macosko, J., Cai, S., Amzel, M., & Ross, C. A. (2002). Huntingtin spheroids and protofibrils as precursors in polyglutamine fibrilization. *Journal of Biological Chemistry, 277*(43), 41032-41037.

Prince, M. J., Wimo, A., Guerchet, M. M., Ali, G. C., Wu, Y.-T., & Prina, M. (2015). World Alzheimer Report 2015-The Global Impact of Dementia: An analysis of prevalence, incidence, cost and trends.

Ramdzan, Y. M., Trubetskov, M. M., Ormsby, A. R., Newcombe, E. A., Sui, X., Tobin, M. J., . . . Miller, J. M. (2017). Huntingtin inclusions trigger cellular quiescence, deactivate apoptosis, and lead to delayed necrosis. *Cell reports, 19*(5), 919-927.

Reginensi, D., Ortiz, D., Pravia, A., Burillo, A., Morales, F., Morgan, C., . . . Gittens, R. A. (2020). Role of Region-Specific Brain Decellularized Extracellular Matrix on In Vitro Neuronal Maturation. *Tissue Engineering Part A, 26*(17-18), 964-978.

Reitz, C. (2013). Dyslipidemia and the risk of Alzheimer's disease. *Current atherosclerosis reports, 15*(3), 307.

Rosén, C., Mattsson, N., Johansson, P. M., Andreasson, U., Wallin, A., Hansson, O., . . . Blennow, K. (2011). Discriminatory analysis of biochip-derived protein patterns in CSF and plasma in neurodegenerative diseases. *Frontiers in aging neuroscience, 3*, 1.

Ruoslahti, E. (1996). Brain extracellular matrix. *Glycobiology, 6*(5), 489-492.

Sachs, P. C., Mollica, P. A., & Bruno, R. D. (2017). Tissue specific microenvironments: a key tool for tissue engineering and regenerative medicine. *Journal of Biological Engineering, 11*(1), 34.

Sahl, S. J., Weiss, L. E., Duim, W. C., Frydman, J., & Moerner, W. (2012). Cellular inclusion bodies of mutant huntingtin exon 1 obscure small fibrillar aggregate species. *Scientific reports, 2*(1), 1-7.

Sakahira, H., Breuer, P., Hayer-Hartl, M. K., & Hartl, F. U. (2002). Molecular chaperones as modulators of polyglutamine protein aggregation and toxicity. *Proceedings of the National Academy of sciences, 99*(suppl 4), 16412-16418.

Sepe, F. N., Chiasserini, D., & Parnetti, L. (2018). Role of FABP3 as biomarker in Alzheimer's disease and synucleinopathies. *Future Neurology, 13*(4), 199-207.

Shi, Y., Sun, X., Sun, Y., Hou, L., Yao, M., Lian, K., . . . Jiang, L. (2016). Elevation of cortical C26: 0 due to the decline of peroxisomal β-oxidation potentiates amyloid β generation and spatial memory deficits via oxidative stress in diabetic rats. *Neuroscience, 315*, 125-135.

Simsa, R., Rothenbücher, T., Gürbüz, H., Ghosheh, N., Emneus, J., Jenndahl, L., . . . Fogelstrand, P. (2021). Brain organoid formation on decellularized porcine brain ECM hydrogels. *PloS one, 16*(1), e0245685.

Soares, T. R., Reis, S. D., Pinho, B. R., Duchen, M. R., & Oliveira, J. M. (2019). Targeting the proteostasis network in Huntington's disease. *Ageing research reviews, 49*, 92-103.

Stoll, E. A., Makin, R., Sweet, I. R., Trevelyan, A. J., Miwa, S., Horner, P. J., & Turnbull, D. M. (2015). Neural Stem Cells in the Adult Subventricular Zone Oxidize Fatty Acids to Produce Energy and Support Neurogenic Activity. *Stem cells, 33*(7), 2306-2319.

Stukel, J. M., & Willits, R. K. (2018). The interplay of peptide affinity and scaffold stiffness on neuronal differentiation of neural stem cells. *Biomedical Materials, 13*(2), 024102.

Thakur, A. K., Jayaraman, M., Mishra, R., Thakur, M., Chellgren, V. M., Byeon, I.-J. L., . . . Conway, J. F. (2009). Polyglutamine disruption of the huntingtin exon 1 N terminus triggers a complex aggregation mechanism. *Nature structural & molecular biology, 16*(4), 380-389.

Thompson, A. J., Pillai, E. K., Dimov, I. B., Foster, S. K., Holt, C. E., & Franze, K. (2019). Rapid changes in tissue mechanics regulate cell behaviour in the developing embryonic brain. *eLife, 8*, e39356.

Walker, F. O. (2007). Huntington's disease. *The Lancet, 369*(9557), 218-228.

Watanabe, A., Toyota, T., Owada, Y., Hayashi, T., Iwayama, Y., Matsumata, M., . . . Ohnishi, T. (2007). Fabp7 maps to a quantitative trait locus for a schizophrenia endophenotype. *PLoS biology, 5*(11), e297.

Yu, A., Shibata, Y., Shah, B., Calamini, B., Lo, D. C., & Morimoto, R. I. (2014). Protein aggregation can inhibit clathrin-mediated endocytosis by chaperone competition. *Proceedings of the National Academy of sciences, 111*(15), E1481-E1490.

Zhang, Y., He, Y., Bharadwaj, S., Hammam, N., Carnagey, K., Myers, R., . . . Van Dyke, M. (2009). Tissue-specific extracellular matrix coatings for the promotion of cell proliferation and maintenance of cell phenotype. *Biomaterials, 30*(23-24), 4021-4028.

Zimmermann, D. R., & Dours-Zimmermann, M. T. (2008). Extracellular matrix of the central nervous system: from neglect to challenge. *Histochemistry and cell biology, 130*(4), 635-653.